

RESEARCH PAPER

Synthesis and Characterization of MFI Zeolite Nanosheets for Optimizing the Dominant Operational Conditions of Methanol to Propylene Process

Naser Hadi¹, Reza Alizadeh^{1*}, Aligholi Niaei²

¹Faculty of Chemical Engineering, Sahand University of Technology, Tabriz, Iran

²Faculty of Chemical Engineering, University of Tabriz, Tabriz, Iran

ARTICLE INFO

Article History:

Received 07 November 2018

Accepted 18 December 2018

Published 01 January 2019

Keywords:

Methanol to Propylene

MFI Zeolite Nanosheet

Neural Network-Genetic

Algorithm

Operational Condition

Optimization

Response Surface Methodology

ABSTRACT

Nanosheets of MFI zeolite were successfully synthesized by hydrothermal method and were properly characterized by XRD, FE-SEM, EDX-dot mapping, TEM, FT-IR, N₂ adsorption/desorption, NH₃-TPD, ICP-AES and TGA techniques. The characterizations of MFI zeolite nanosheets suitably confirmed well synthesized MFI nanostructure, superior specific surface area (695.96m².g⁻¹) and great mesopores volume. Currently, the major concern in commercialized technologies of methanol to propylene (MTP) process is to discover the best operational conditions for maximizing propylene selectivity. Therefore, in present investigation the effectiveness of more significant operational conditions such as reaction temperature, methanol molar percent in feedstock and methanol WHSV on propylene selectivity was considered. For first time, conventional response surface methodology and an artificial neural network model coupled with genetic algorithm were appropriately employed to optimize MTP operational conditions. For providing the data bank of optimization, MTP reaction was carried out over the synthesized MFI zeolite nanosheets at various operational conditions. It was concluded that neuro-genetic method showed more reliable performance in optimizing MTP operational conditions with R² value of 0.9998. Furthermore, time on stream examination was conducted over MFI zeolite nanosheets at optimal operational conditions which were suggested by neuro-genetic approach. At optimal operational conditions the catalytic life-time was sufficiently enhanced (101h).

How to cite this article

Hadi N, Alizadeh R, Niaei A. Synthesis and Characterization of MFI Zeolite Nanosheets for Optimizing the Dominant Operational Conditions of Methanol to Propylene Process. J Nanostruct, 2019; 9(1): 51-73. DOI: 10.22052/JNS.2019.01.007

INTRODUCTION

Because of growing demand for light olefins especially propylene, the petrochemicals should appropriately respond to the market requirements [1, 2]. Selective production of propylene from methanol (MTP reaction) is a promising technology that converts coal, natural gas and biomass [3, 4] to the valuable products via methanol as an intermediate material [5, 6]. The MTP reaction has some economical advantages. The feed of the MTP (methanol) is a cheap, available alcohol

in comparison with other feedstock for producing light olefins [7, 8]. Large amounts of methanol are produced annually via synthesis gas which is obtained by steam reforming of natural gas [5, 9, 10]. The conversion of methanol in the MTP reaction is high (near 99%) [7, 11-19] and the sole concern is to improve the MTP catalysts for enriching the propylene selectivity. More than 50 mol% of product contribution of the MTP process belongs to the strategic monomer of propylene [18]. Furthermore, the MTP reaction is carried out

* Corresponding Author Email: r.alizadeh@sut.ac.ir

at atmospheric pressure which reduces the costs of process equipment [20]. More freshly, Ortiz-Espinoza et al. [21] carried out an economic, energy and environmental evaluation for the Oxidative Coupling of Methane (OCM) and the Methanol to Olefins (MTO) processes in producing of ethylene. The findings represented that the MTO process is more profitable from the economic and technical point of view.

According to the literature survey, numerous investigations have been examined for development of the MTP/MTO processes at different operating conditions [22]. But none of them optimized the parameters of the operating conditions in a systematic method in order to maximize the propylene selectivity. For example, Wu et al. [23] investigated the MTO reaction in an isotherm fixed-bed reactor at different methanol partial pressures, water/methanol ratios and reaction temperatures over H-ZSM-5 catalyst. It was found that product distribution was remarkably affected by the mentioned operational conditions. Zhuang et al. [24] developed a combined discrete element method (DEM) and computational fluid dynamics (CFD) model for the MTO process. The influences of operating conditions on product distribution were also studied. It was resulted that the reaction temperature, inlet gas velocity and feed ratio of water to methanol meaningfully affected the reaction productivity. All of the investigations which were mentioned above and some others [13, 15, 17, 25-30] carried out the MTP/MTO reaction without optimizing the operating conditions. Limited researchers optimized the operating conditions of the MTP/MTO processes. Ghavipour et al. [31] synthesized the H-ZSM-5 catalyst and examined it in the methanol to hydrocarbons (MTHC) reaction. The effect of reaction temperature and water dilution on product distribution was investigated with one factor at a time strategy [31]. Najafabadi et al. [32] investigated the MTO process over the SAPO-34 catalyst. They studied effect of the dominant operating conditions such as reaction temperature, water to methanol molar ratio in feedstock and methanol space time on product distribution. The optimization of operating conditions was carried out by Najafabadi et al. [32] without using any intelligent method. Hajimirzaee [33] conducted the dehydration of methanol to light olefins over a mixture of zeolite/alumina catalyst. The influence of more important operating conditions such as

reaction temperature, feed space velocity and feed composition on conversion of methanol to light olefins was considered. But the reaction factors were changed by trial and error and a coherent procedure for optimizing the operating conditions was lacking.

Determination of the optimal operating conditions for the MTP reaction is a hard work containing elaborated interactions between various parameters. Therefore, the experiments for definition of the optimal operating conditions are prolonged, expensive and tedious. Nowadays, black-box modeling and intelligent methods such as conventional Response Surface Methodology (RSM), Central Composite Design (CCD), Artificial Neural Network (ANN) and Genetic Algorithm (GA) have been developed for optimizing the chemical processes [34-36]. The intelligent approaches create a systematic search in the wide-spread parameter space [37]. They also decrease the number of experiments and obtain the optimal conditions of a chemical process more efficiently [16, 38-46]. These intelligent optimization methods were extensively used in the literature for waste water treatments, air pollution, environmental issues and other chemical reactions and processes [41, 47-52]. For instance, Sedighi et al. [53] studied the effect of reaction temperature, space time and the molar ratio of morpholine to alumina over the SAPO-34 catalyst in MTO reaction. RSM was employed to examine the influence of main factors and their interactions. It was concluded that the effects of reaction temperature and space time were the key factors on light olefins yield. Hadi et al. [16, 54] synthesized the M-Mn/H-ZSM-5 (M: Cr, Ce, Fe, Ni) bimetallic catalysts for selective formation of propylene from methanol. The main factors of wt.% of second metal loading, calcination temperature, calcination time and the atomic descriptors of second metal were optimized by conventional RSM-CCD and ANN-GA integrated approaches. The aim of optimization was to enrich the propylene selectivity. Adib et al. [55] utilized an ANN model to predict the molar percent of CH₄, CO₂ and CO in the Fischer-Tropsch (FTS) process of natural gas. The GA optimizer was employed to obtain the optimal operational parameters. The results showed that the combinatorial ANN-GA technique could be successfully used for FTS process as an influential method. Ghorbani et al. [56] used a hybrid ANN-GA for predicting viscosity of Iranian crude oils. It was found that these

models were very appropriate approximations for estimating the viscosity of Iranian crude oils.

The catalytic conversion of methanol to propylene is generally carried out over the MFI type zeolites. A novel morphology of the MFI zeolite has been synthesized which is known as MFI zeolite nanosheets [57-63]. The MFI zeolite nanosheets proved greater activity and higher selectivity to propylene in comparison with the referenced conventional H-ZSM-5 catalyst [61, 64]. More recently, Hadi et al. [65] hydrothermally synthesized the nanosheets of M-substituted (M: Mn, Ce, W) MFI type zeolites. The nanosheets of W-substituted MFI zeolite represented the best performance in the MTP reaction.

As it was earlier mentioned, regarding to the available literature the optimization of the key operating conditions of the MTP reaction by intelligent methods was not previously implemented. Hence in the current work, for maximizing the propylene selectivity, the main parameters of operating conditions of the MTP reaction such as reaction temperature, methanol molar percent in feedstock and WHSV of methanol were elucidated by both of the conventional RSM coupled with CCD and a combinatorial smart technique named neuro-genetic approach. The neuro-genetic approach was developed by our research group to optimize the variables in different chemical processes [40-44, 54]. The MTP reaction was carried out over the MFI zeolite nanosheets which were synthesized by hydrothermal method. The activity of the MFI zeolite nanosheets was examined at specific operating conditions which were determined by experimental design. Also, some catalyst examinations were conducted at desired operational conditions over the synthesized MFI zeolite nanosheets. By evaluating the performance of MFI zeolite nanosheets at particular operating conditions, the experimental data were collected and the ANN model of the operating conditions was developed. The ANN model was utilized as a fitness function of GA for finding the optimal operating conditions.

MATERIALS AND METHODS

The starting materials for synthesis of the special bifunctional organic surfactant ($C_{22-6-6}Br_2$) were as follows: 1-bromodocosane (96 wt.%), N,N,N',N'-tetramethyl-1,6-hexanediamine (99 wt.%), 1-bromohexane (98 wt.%), toluene (98 wt.%),

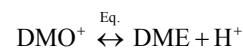
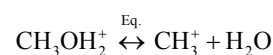
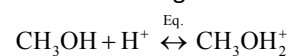
acetonitrile (98 wt.%), diethyl ether (98 wt.%) and materials needed to prepare the synthetic gel of the MFI zeolite nanosheets were: tetraethyl ortho silicate (99 wt.%), sodium hydroxide (98 wt.%), sulphuric acid (98 wt.%), aluminum sulphate (98 wt.%) and ammonium chloride (98 wt.%). All of the materials were extra pure provided by Merck and Aldrich corporations.

Synthesis of MFI zeolite nanosheets

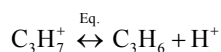
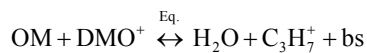
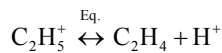
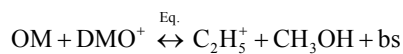
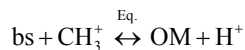
The diquaternary ammonium-type surfactant of $C_{22}H_{45}-N^+Br^-(CH_3)_2-C_6H_{12}-N^+Br^-(CH_3)_2-C_6H_{13}$ was synthesized according to the modified methods advised by Choi et al. [57] and Machoke et al. [60]. The synthesized special bifunctional organic surfactant was identified as $C_{22-6-6}Br_2$. It was utilized as structure directing agent (SDA) for synthesis of the MFI zeolite nanosheets. The MFI zeolite nanosheets were synthesized via hydrothermal method according to the modified procedure [57, 58, 60, 65]. The optimal molar composition for preparing the synthetic gel was: 30 Na_2O : 100 SiO_2 : 0.2 Al_2O_3 : 10 $C_{22-6-6}Br_2$: 18 H_2SO_4 : 4000 H_2O . The optimal molar composition was proposed by Machoke et al. [60]. The molar composition was regulated to obtain the MFI zeolite nanosheets with Si/ Al_2 ratio of 500. The procedure of gel preparation was comprehensively explained in our previous work [65].

Reaction mechanism and process set up for catalyst examinations

The activity of the MFI zeolite nanosheets was examined in a vertical fixed bed reactor under atmospheric pressure. In the MTP reactor, methanol is dehydrated into the equilibrium mixture of methanol, dimethyl ether (DME) and water according to the following reactions:



where, H^+ , $CH_3OH_2^+$, CH_3^+ and DMO^+ determine acidic site of zeolite, methoxonium ion, surface methoxy and dimethyl oxonium ion, respectively. DME is an intermediate in the MTP reaction. Subsequently, the light olefins are formed via the following reactions [66, 67]:



where, bs, OM, C_2H_5^+ and C_3H_7^+ indicate the basic site of zeolite, oxonium methylide, ethyl carbenium ion and propyl carbenium ion, respectively. Consecutively, higher olefins, alkanes, cyclo alkanes and aromatics are generated via methylation, hydrogen transfer, oligomerization and aromatization (cyclization) reactions. Numerous mechanisms were suggested for interpreting these reactions but it seems that the dual-cycle reaction mechanism which was proposed by Bjørgeren et al. [68] is more dependable mechanism for the MTP/MTO reaction [69]. Fig. S1 depicted the dual-cycle mechanism which is contained two main cycles: the cycle of aromatic and the cycle of alkene formations. For the aromatic cycle, the cations of methylcyclopentenyl (MCP^+) and polymethyl-benzenium (polyMB^+) are the major active intermediates [70-72]. For the alkene cycle, the methylation and cracking reactions of C_3^- - C_7^- straight chain alkenes are occurred [73, 74]. In the dual-cycle mechanism, the two main cycles considerably influence on each other. The olefins which are generated by the aromatic cycle can play a significant role as the active intermediates in the alkene cycle. The reaction of hydrogen transfer links the two main cycles as a side reaction. Hydrogen transfer converts the heavy olefins to the saturated higher alkanes in the alkene cycle and also converts the heavy olefins to the aromatics and the other unsaturated cyclic hydrocarbons in the aromatic cycle [75, 76].

The MTP products were analyzed by Shimadzu® 2010 plus model gas chromatograph (GC). Fig. S2 displayed the schematic flow diagram of the experimental set up.

Techniques of catalyst characterization

The structure of the MFI zeolite nanosheets was characterized with powder X-Ray Diffraction (XRD) by a Siemens® D500 X-ray diffractometer. The technique of Field Emission Scanning

Electron Microscopy (FE-SEM) was employed for determining the surface morphology of catalyst. The FE-SEM image was registered on a MIRA3 TESCAN® microscope. For qualitative elemental analysis of MFI zeolite nanosheets, the Energy Dispersive X-ray (EDX) technique was employed. Transmission Electron Microscopy (TEM) images were recorded from the ultrathin edges of sheets along the *b*-crystal axis (i.e., perpendicular to the nano-layers) and also the surface of sheets of MFI zeolite. For TEM, the catalyst sample was supported on a holey carbon coated grid Cu mesh 300. TEM images were taken by Zeiss EM10C equipment operated at 100 kV. In order to determine the surface functional groups, the Fourier Transform Infrared (FT-IR) technique was utilized with a Tensor 27- Bruker® spectrometer. The N_2 adsorption/desorption technique was conducted by NOVA2000 Quanta Chrome USA system to disclose the textural properties of MFI zeolite nanosheets. The surface acidity of MFI zeolite nanosheets and the referenced conventional H-ZSM-5 was investigated by Temperature Programmed Desorption of ammonia (NH_3 -TPD) with a BELCAT-A, BEL Japan, Inc. device. The real compositions of Si and Al species in the catalyst sample were specified by Inductively Coupled Plasma-Atomic Emission Spectrometry (ICP-AES). It was carried out by IRIS advantage ICAP full spectrum direct-reading emission spectrometer (TJA Solutions, USA). Thermo Gravimetric Analysis (TGA) was utilized to reveal the amounts of coke deposition on the MFI zeolite nanosheets after the life-time examination. For this purpose, temperature was increased at a constant rate of 10 °C/min to 800 °C under flowing air employing Perkin Elmer (RIS Diamond), thermal analysis apparatus. The sample weight loss resulting from the reaction of deposited coke by oxygen was recorded.

COMPUTATIONAL APPROACH

Response surface methodology

The significance and principals of conventional RSM were thoroughly expressed in our previous work [54]. The conventional RSM is useful to analyze chemical systems [77-79]. In order to design the experiments, the central composite design (CCD) was used. The significant advantage of the CCD is that it does not offer large number of design points [45, 80]. Due to formulate the parameters, the following quadratic model was

employed:

$$y = \beta_0 + \sum_{i=1}^k \beta_i x_i + \sum_{i=1}^k \beta_{ii} x_i^2 + \sum_{i < j} \beta_{ij} x_i x_j + \varepsilon \quad (1)$$

Where, y , β_0 , k , β_i , β_{ii} , β_{ij} , x_i , x_j and ε are the predicted response (propylene selectivity), constant coefficient, factor numbers, linear coefficients, quadratic coefficients, interaction coefficients, coded values of parameters and the error, respectively.

Artificial neural network model

For comparing the optimized operational conditions which were acquired by the conventional RSM, an intelligent optimization method known as the neuro-genetic approach or the ANN-GA hybrid system was utilized. The experimental data based on the CCD plus the supplementary empirical data were employed as the experimental data bank for combinatorial neuro-genetic method. The topology of the ANN was organized by multilayer perceptron (MLP). The number of input neurons in the ANN model was associated with the number of operating condition factors. The number of neurons in hidden layer is changed for different problems. For discovering the optimal number of neurons in hidden layer, the network was developed by inserting neurons to the hidden layer until the best result was achieved. The hyperbolic tangent sigmoid was applied as the transfer function for neurons of hidden layer. The weights of neurons were trained by method of gradient descend with momentum back propagation (traingdm). The selectivity to propylene was considered as the output of the ANN model. The propylene selectivity represented the catalytic activity of the MFI zeolite nanosheets at distinctive operating conditions. For predicting the maximum propylene selectivity, the optimal ANN topology was linked with GA. The correlation coefficient (R^2) and the Root Mean Square Error (RMSE) were used to compare the sufficiency of ANN topologies.

$$R^2 = 1 - \frac{\sum_{i=1}^n (MO_i - EO_i)^2}{\sum_{i=1}^n (EO_i - \overline{EO_i})^2} \quad (2)$$

$$RMSE = \sqrt{\frac{1}{n} \sum_{i=1}^n (MO_i - EO_i)^2} \quad (3)$$

where MO_i is the model output for i^{th} experiment, EO_i is the experimental output data of the propylene selectivity, $\overline{EO_i}$ is the mean of experimental output data and n is the total number of experiments. The effect of each input factor on the output factor, was calculated by Eq.4 [81]. Eq.4 determines the model sensitivity to each input factor.

$$S_s = \frac{\sum_{j=1}^n \frac{w_{sj} u_{jk}}{\sum_{i=1}^m w_{ij}}}{\sum_{i=1}^m \sum_{j=1}^n \frac{w_{ij} u_{jk}}{\sum_{i=1}^m w_{ij}}} \quad (4)$$

where S_s is the effect of s^{th} input factor, w_{ij} is the weight that connects the i^{th} input to the j^{th} neuron of hidden layer, u_{jk} is the weight which links j^{th} neuron of hidden layer to k^{th} output neuron, m is the number of input neurons (number of operational condition factors), n is the number of neurons in hidden layer, and k is the number of network outputs which equals to 1 in the current investigation.

Genetic algorithm optimizer

For elucidating the optimal operational conditions of the MTP reaction, the optimal ANN topology was coupled with the GA. The GA generated virtual operating conditions of the MTP reaction and the ANN model functioned as a virtual catalyst examination set up at specified operating conditions which evaluated the fitness of GA. In the present study, each chromosome of genetic algorithm contained three genes identifying the parameters of main operational conditions. The flowchart of optimization process by neuro-genetic method was represented in Fig. 1. The optimization was conducted by codes of ANN coupled with GA codes in MATLAB®. Table 1 shows the optimal parameters of the GA. Other parameters were held at their default values or types.

RESULTS AND DISCUSSION

Catalyst characterization

The structure of the MFI zeolite nanosheets was investigated by the XRD pattern. For comparing, the structure of the referenced MFI type zeolite (H-ZSM-5) was also studied by the XRD (Fig. 2). The XRD analyses proved two individual sharp peaks at 2θ of 8-10° and 20-25°. Both of these sharp peaks associated with the referenced MFI type zeolite

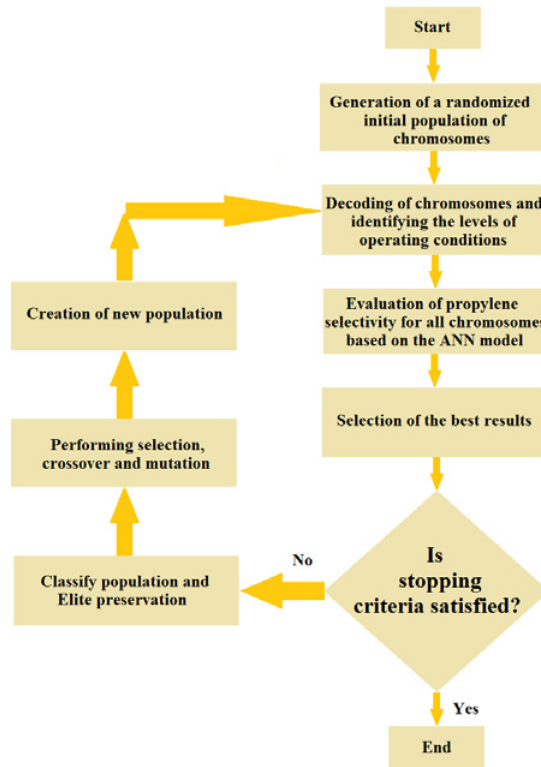


Fig. 1. The flowchart of optimization procedure using neuro-genetic approach

Table 1. Important factors of genetic algorithm which were employed in optimization process

Factor	Value or type	Factor	Value or type
Population type	Double vector	Elite count	2
Population size	100	Mutation function	Gaussian
Generation	100	Selection function	Stochastic uniform
Crossover fraction	0.8	Crossover function	Scattered
Fitness scaling	Rank	Hybrid function	Fminsearch

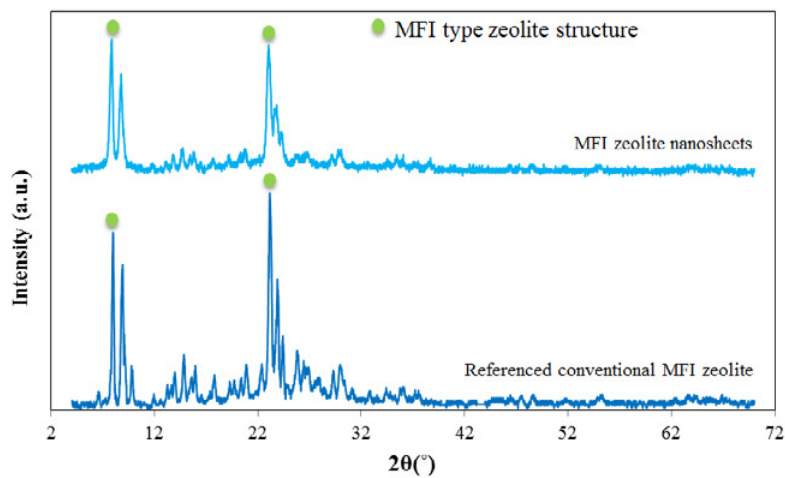


Fig. 2. XRD patterns of the referenced conventional MFI zeolite (H-ZSM-5) and nanosheets of MFI zeolite; Circles determined the MFI type zeolite crystal structure

with regard to the JCPDS (Joint Committee on Powder Diffraction Standards) data [82]. According to the referenced MFI zeolite, no considerable alteration in phase was detected in the structure of MFI zeolite nanosheets. Only the intensity of the characteristic peaks was somewhat declined for nanosheets of MFI zeolite. It was related to

the lower amount of Al atoms in structure of MFI zeolite nanosheets.

FE-SEM image illustrated the surface morphology of the MFI zeolite nanosheets (Fig. 3). The FE-SEM image verified that the catalyst sample was included from the ultrathin MFI zeolite nanolayers. The nanosheets of MFI zeolite showed relatively uniform thicknesses. It was resulted that the nanosheets of MFI zeolite were properly synthesized.

The qualitative elemental analysis was carried out with EDX-dot mapping method in order to prove the existence of required components and also to show the distribution of chemical species in the lattice of catalyst sample. Fig. 4 denoted the EDX-dot mapping graph of the MFI zeolite nanosheets. The results demonstrated the presence of desired components and suitable dispersion of various chemical species in framework of MFI zeolite nanosheets.

Fig. 5 represented TEM images of the synthesized catalyst sample. Fig. 5a were taken from the ultrathin edges of sheets along the *b*-crystal axis and confirmed that the catalyst sample were structured from the ultrathin MFI

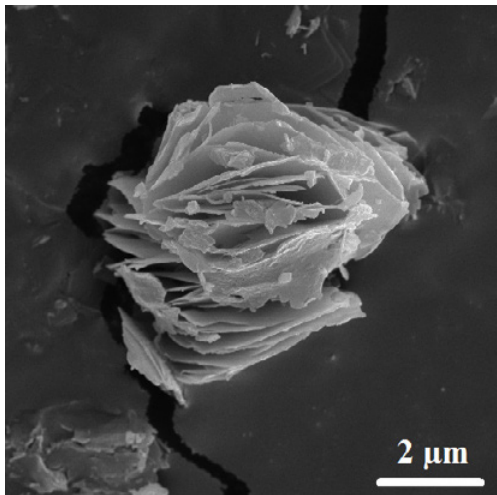


Fig. 3. FE-SEM image of the high silica MFI zeolite nanosheets with Si/Al₂ ratio of 500

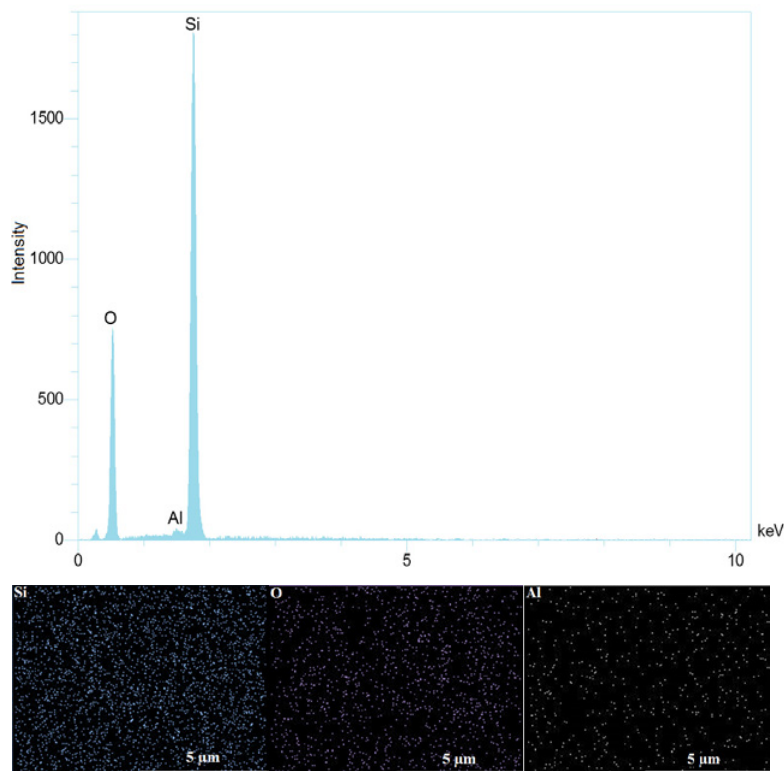


Fig. 4. EDX-dot mapping graph of high silica MFI zeolite nanosheets with Si/Al₂ ratio of 500

zeolite sheets with relatively uniform nano-scale thicknesses. Similarly, Fig. 5(b, c) were recorded from the surface of sheets of MFI zeolite and verified that they were consisted of ultrafine crystals. In consistent with the FE-SEM image, it was concluded by TEM images that the nanosheets of MFI zeolite were successfully synthesized according to the nano-scale thicknesses of the MFI zeolite layers. The ultrathin layers of MFI zeolite appropriately shorten the diffusion path for both of the reactants and products in the MTP reaction. Therefore, the unwanted reactions

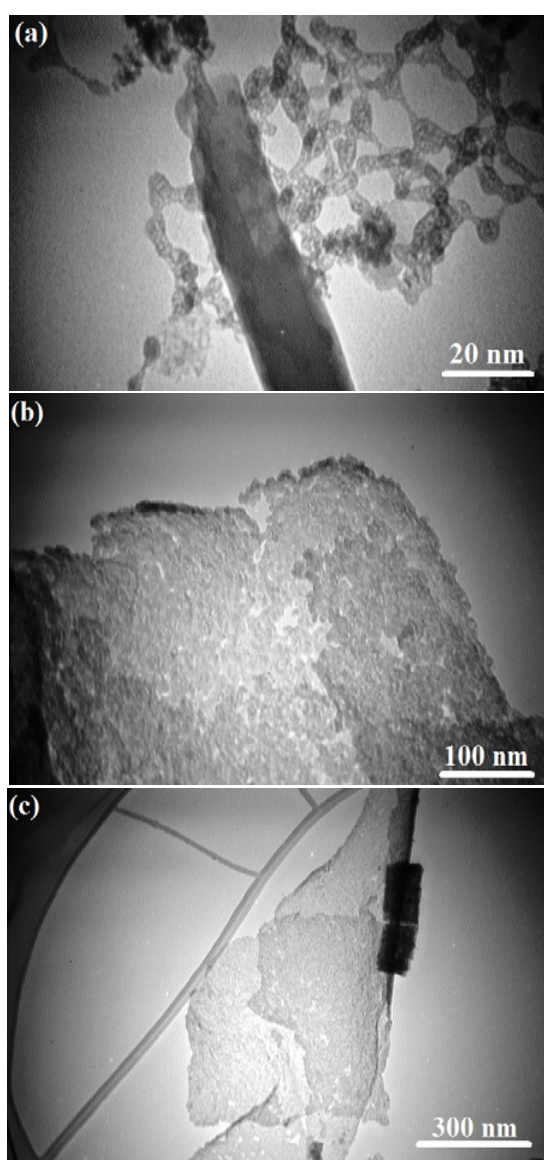


Fig. 5. TEM images of high silica MFI zeolite nanosheets with Si/Al₂ ratio of 500; a) the edges of MFI zeolite sheets, b) and c) the surfaces of MFI zeolite sheets

like aromatization, oligomerization and hydrogen transfer are considerably prevented, leading to greater selectivity to light olefins especially propylene.

Fig. 6 displayed the FT-IR spectra of the MFI zeolite nanosheets and the referenced conventional H-ZSM-5 in the wavenumber range of 400-4000 cm⁻¹. As evidenced by Fig. 6, the characteristic peaks of the referenced MFI type zeolite (H-ZSM-5) were also identified by the nanosheets of MFI zeolite.

The total specific surface area (S_{BET}), mesopore area (S_{Meso}), total pore volume (V_{Total}) and mesopore volume (V_{Meso}) of the MFI zeolite nanosheets were 695.96 m².g⁻¹, 451.02 m².g⁻¹, 0.904 cm³.g⁻¹ and 0.731 cm³.g⁻¹, respectively. All of the mentioned textural properties of MFI zeolite nanosheets were much greater than that of the referenced conventional H-ZSM-5 [65]. The superior activity of nanosheets in the MTP reaction is attributed to their unique morphology and exceptional textural properties including high specific surface area and great mesoporosity [61].

The acidity of the MFI zeolite nanosheets and the referenced conventional H-ZSM-5 was determined by NH₃-TPD analysis (Fig. 7). According to Fig. 7, the lower peak at 170-200 °C was related to the NH₃ desorption from weak acidic sites whereas the higher peak at 250-320 °C was attributed to the NH₃ desorption from strong acidic sites. In the MTP reaction, too much of strong acidic sites accelerate the side reactions. While the fewer strong and weak acidic sites of catalyst facilitate the generation of initial C-C bond by alkylation and methylation reactions which positively enhance propylene production. As supported by Fig. 7, the strength of acidic sites predominantly the strong acidic sites were weakened more for the MFI zeolite nanosheets in comparison with the referenced conventional H-ZSM-5.

The ICP-AES technique was used to investigate the quantitative elemental composition of the MFI zeolite nanosheets. It was deduced that the Si/Al₂ ratio of the MFI zeolite nanosheets was about 488 which was associated with its nominal Si/Al₂ ratio (500).

Investigation of main operational conditions

The aim of present investigation was to determine the optimal operational conditions for accelerating the alkene cycle (Fig. S1) to produce more propylene. In other words, the purpose

of current work was to clarify the optimized operational conditions of the MTP reaction by RSM-CCD and the combinatorial neuro-genetic technique, for maximizing the response of system. The response of system was propylene selectivity which was obtained at different operational conditions over the synthesized MFI zeolite nanosheets. Main factors of operational conditions and their levels in the experimental design (CCD) were reported in Table 2. The lower and upper bounds of operational conditions were defined by preliminary examinations based on literature

survey [14]. For better training of the ANN model, the supplementary MTP examinations at desired operational conditions were also carried out over the nanosheets of MFI zeolite. The results of MTP reaction at various operational conditions were tabulated in Table 3.

Generally, the MTP reaction pathway is affected by the amounts of methanol conversion. At lower methanol conversion the concentration of methanol and DME in the reaction zone is high and methylation reaction is prominent. Meanwhile, at higher methanol conversions

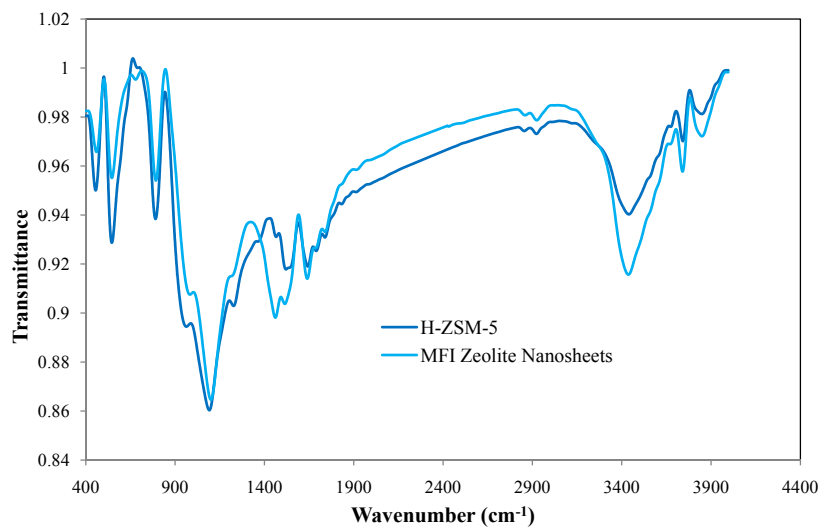


Fig. 6. FT-IR spectra of referenced conventional MFI zeolite (H-ZSM-5) and MFI zeolite nanosheets

Table 2. Matrix of experimental design based on CCD, experimental response and predicted values by RSM

Run Order	Coded variable			Natural variable			Response: Propylene selectivity (%)	
	Reaction temp. (°C)	Mol. % of methanol	WHSV of methanol (h ⁻¹)	Reaction temp. (°C)	Mol. % of methanol	WHSV of methanol (h ⁻¹)	Experiment	Predicted by RSM
1	0	-1.5	0	400	5	2.5	41.40	40.99
2	0	0	0	400	50	2.5	50.01	50.09
3	0	1.5	0	400	95	2.5	46.32	45.89
4	0	0	0	400	50	2.5	50.00	50.09
5	1	-1	1	500	20	4.1	45.22	45.89
6	0	0	0	400	50	2.5	49.99	50.09
7	-1	-1	1	300	20	4.1	38.62	38.66
8	-1.5	0	0	250	50	2.5	44.46	44.52
9	1	1	-1	500	80	0.9	46.99	47.42
10	0	0	1.5	400	50	4.9	48.08	47.33
11	1	-1	-1	500	20	0.9	44.12	44.23
12	1	1	1	500	80	4.1	48.32	48.68
13	0	0	0	400	50	2.5	49.95	50.09
14	-1	1	1	300	80	4.1	41.64	42.00
15	0	0	-1.5	400	50	0.1	45.17	45.08
16	0	0	0	400	50	2.5	49.97	50.09
17	1.5	0	0	550	50	2.5	50.87	50.04
18	0	0	0	400	50	2.5	49.98	50.09
19	-1	1	-1	300	80	0.9	40.87	40.67
20	-1	-1	-1	300	20	0.9	36.82	36.93

the content of methanol and DME is lower and olefins concentration is greater. In that case, the olefins oligomerization and cracking reactions are prevailing [83]. It was concluded that olefin methylation reactions and cracking of heavy olefins to light olefins take place at the same time [84]. Hence, the dominant reaction scheme in MTO/MTP processes at lower methanol conversions is that light olefins are methylated by methanol from butylene through pentene to hexene and further to heptene which crack to generate light olefins (ethylene and propylene) again [13, 85]. Methylation reactivity of ethylene and propylene is enormously low and it can be ignored [86]. Eventually, a steady state distribution of olefins is resulted by the equilibrium reactions

of methylation and cracking. As it was previously mentioned, the olefins concentration is much greater than methanol at superior methanol conversions and conjugate oligomerization/cracking reactions are prominent leading to the cracking of heavy hydrocarbons to light ones. This issue is agreed with our empirical data that at higher methanol conversions the propylene selectivity is also high but the selectivity to C₅⁺ hydrocarbons is low (Fig. 8-Fig. 10).

The influence of reaction temperature

The influence of reaction temperature on methanol conversion to olefins over the ZSM-5 zeolite (MFI type zeolite) has been extensively reported [87, 88]. It is generally known that

Table 3. Supplementary experimental data for propylene selectivity which were obtained at different MTP operational conditions over the synthesized nanosheets of MFI zeolite

Run order	Reaction temp. (°C)	Mol. % of methanol	WHSV of methanol (h ⁻¹)	Propylene selectivity (%)	Run order	Reaction temp. (°C)	Mol. % of methanol	WHSV of methanol (h ⁻¹)	Propylene selectivity (%)
1	260	2	2.60	28.76	45	360	50	1.00	40.37
2	310	2	2.60	31.76	46	410	50	1.00	42.17
3	360	2	2.60	35.16	47	460	50	1.00	44.44
4	410	2	2.60	37.20	48	510	50	1.00	44.85
5	460	2	2.60	40.40	49	560	50	1.00	44.70
6	510	2	2.60	38.80	50	260	50	4.00	40.58
7	560	2	2.60	37.10	51	310	50	4.00	42.88
8	260	30	2.60	44.09	52	360	50	4.00	45.37
9	310	30	2.60	47.10	53	410	50	4.00	46.87
10	360	30	2.60	50.56	54	460	50	4.00	49.56
11	410	30	2.60	52.70	55	510	50	4.00	48.96
12	460	30	2.60	55.00	56	560	50	4.00	48.77
13	510	30	2.60	53.65	57	260	50	5.00	39.88
14	560	30	2.60	52.00	58	310	50	5.00	40.75
15	260	50	2.60	42.26	59	360	50	5.00	43.18
16	310	50	2.60	45.56	60	410	50	5.00	45.47
17	360	50	2.60	48.89	61	460	50	5.00	47.88
18	410	50	2.60	51.10	62	510	50	5.00	47.58
19	460	50	2.60	54.30	63	560	50	5.00	47.12
20	510	50	2.60	52.45	64	460	2	0.08	29.47
21	560	50	2.60	50.78	65	460	18	0.08	36.89
22	260	82	2.60	39.21	66	460	30	0.08	42.49
23	310	82	2.60	41.51	67	460	66	0.08	39.76
24	360	82	2.60	44.84	68	460	82	0.08	37.41
25	410	82	2.60	46.05	69	460	98	0.08	36.98
26	460	82	2.60	49.15	70	460	2	1.00	32.24
27	510	82	2.60	47.39	71	460	18	1.00	39.54
28	560	82	2.60	45.62	72	460	30	1.00	45.75
29	260	98	2.60	35.53	73	460	66	1.00	42.61
30	310	98	2.60	39.83	74	460	82	1.00	39.86
31	360	98	2.60	43.10	75	460	98	1.00	39.69
32	410	98	2.60	44.85	76	460	2	4.00	37.45
33	460	98	2.60	48.95	77	460	18	4.00	44.97
34	510	98	2.60	46.18	78	460	30	4.00	50.23
35	560	98	2.60	44.53	79	460	66	4.00	47.81
36	260	50	0.08	33.55	80	460	82	4.00	46.02
37	310	50	0.08	35.75	81	460	98	4.00	45.65
38	360	50	0.08	38.37	82	460	2	5.00	34.97
39	410	50	0.08	40.17	83	460	18	5.00	42.86
40	460	50	0.08	41.69	84	460	30	5.00	48.73
41	510	50	0.08	42.18	85	460	66	5.00	46.27
42	560	50	0.08	42.59	86	460	82	5.00	44.52
43	260	50	1.00	34.55	87	460	98	5.00	43.73
44	310	50	1.00	37.75	88	460	66	2.60	52.49



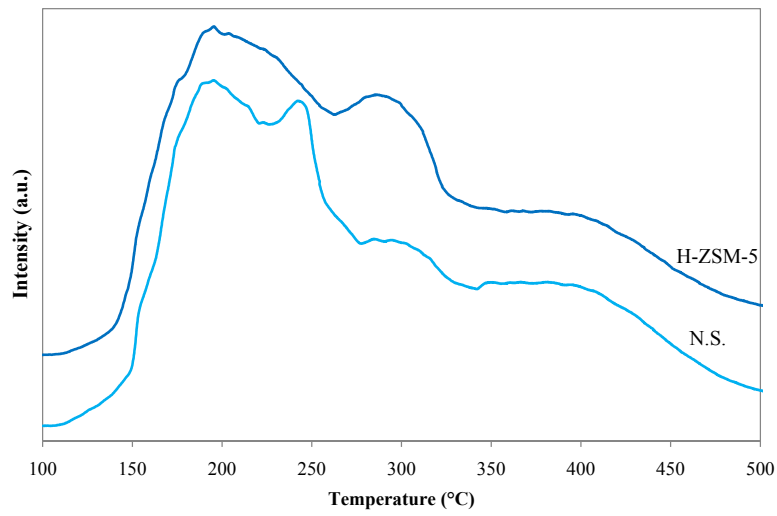


Fig. 7. NH_3 -TPD profiles of referenced conventional H-ZSM-5 and (N.S.): MFI zeolite nanosheets

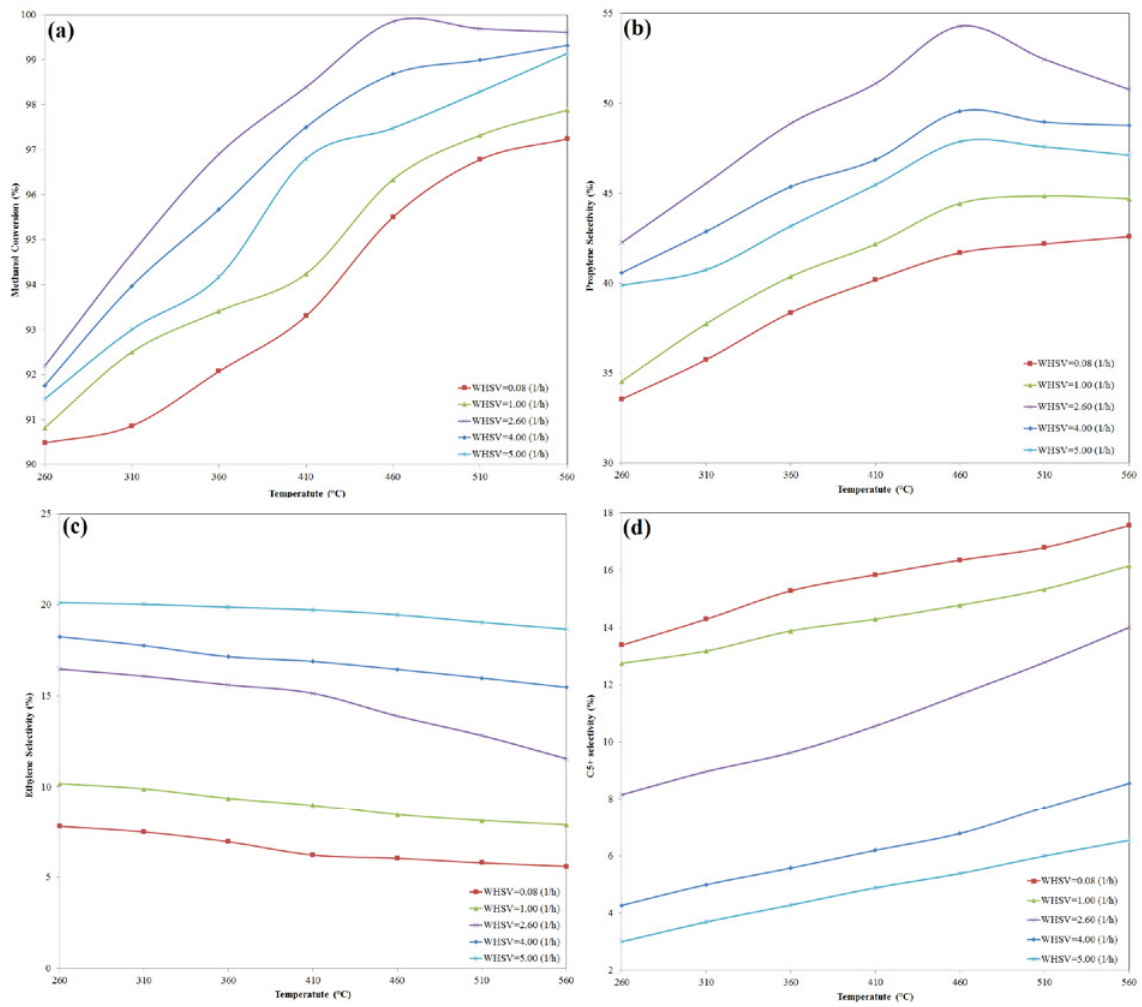


Fig. 8. Simultaneous influence of reaction temperature and methanol WHSV on methanol conversion and selectivity to main MTP products at constant methanol molar percent of 50%

methanol conversion and propylene selectivity are enriched at higher reaction temperatures (450-500 °C). In the MTP process, the reaction temperature should not be exceeded from 570 °C. Because according to the dual-cycle reaction mechanism (Fig. S1), the higher reaction temperature provides the activation energy of side reactions in the aromatic cycle such as hydrogen transfer, oligomerization and aromatization (cyclization) reactions. These secondary reactions produce the side products like heavy alkanes, cycloalkanes and aromatics. This subject unwantedly reduces the propylene selectivity in the MTP reaction. Moreover, the high reaction temperature causes sintering of the catalyst particles because of creation the hot spots in the reactor which decrease the number of active sites of the catalyst.

Fig. 8 illustrated the effect of reaction temperature on the methanol conversion and selectivity to main MTP products at various methanol WHSVs and constant methanol molar percent of 50% in feedstock. Likewise, the results

of experimental data which were obtained at certain operational conditions proposed by CCD were displayed by Fig. S3. The Fig. S3(a-d) and Fig. S3(e) showed the selectivity of MTP products and mole percent of unconverted methanol at 300 and 500 °C and at 250, 400 and 550 °C, respectively with constant values of methanol molar percent in feedstock and methanol WHSV.

According to Fig. 8a increasing reaction temperature leads to the higher methanol conversions at the same WHSV. Whenever the reaction temperature reduces from 460 °C to 360 °C, approximately fourfold more WHSV is needed to hold the same methanol conversion. As evidenced by Fig. 8b the propylene selectivity shows almost the similar trend with the methanol conversion. The propylene selectivity is maximized at reaction temperature of 460 °C and WHSV of 2.6 h⁻¹. At higher reaction temperatures than 460 °C, the propylene selectivity is somewhat decreased probably because of prevailing the methylation reactions of light olefins to higher hydrocarbons

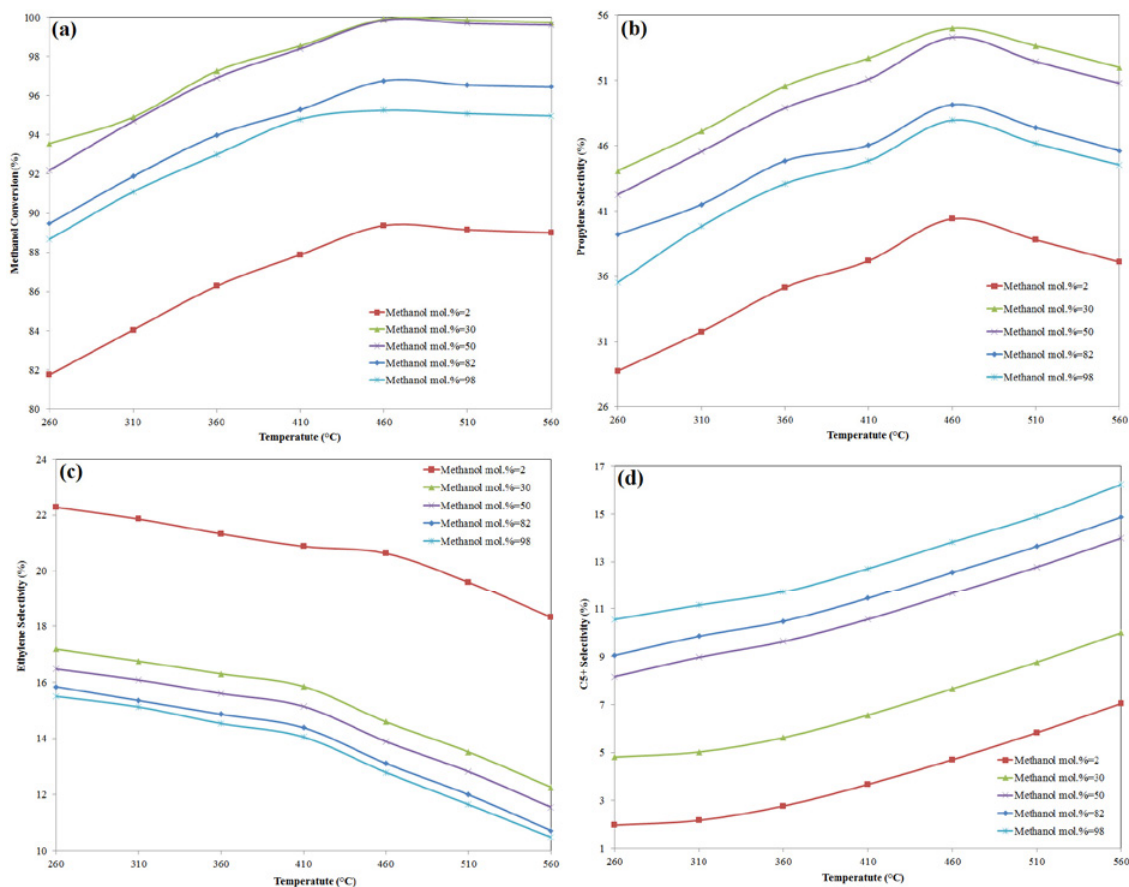


Fig. 9. Simultaneous effect of reaction temperature and methanol molar percent on methanol conversion and selectivity to main MTP products at constant methanol WHSV of 2.6 h⁻¹

(C_5^+). This issue is also confirmed by Fig. 8d where the selectivity to C_5^+ hydrocarbons increases steadily with reaction temperature especially, it is intensified at higher reaction temperatures (460-560 °C). Fig. 8c exhibits slight reduction in ethylene selectivity with increasing reaction temperature. It approves the low methylation reactivity of ethylene by varying the reaction temperature. Similarly, as evidenced by Fig. S3(a-e), increasing the reaction temperature enhances the methanol conversion and selectivity to propylene, butylene and C_5^+ hydrocarbons while, slightly reduces the selectivity to C_1 - C_4 alkanes and ethylene. Therefore, the higher reaction temperatures are more suitable for enriching the propylene selectivity. Altogether, it can be concluded that the higher reaction temperatures modify the catalytic activity as well as the selectivity to the heavy hydrocarbons

[32]. At higher reaction temperatures, the rate of methylation and cyclization reactions increase which cause to create the heavy hydrocarbons from the light ones. As it is clear in Fig. 8(a-b), the methanol conversion and propylene selectivity are enriched near reaction temperature of 460 °C.

The effect of methanol molar percent in feedstock

Water is inserted in feedstock of the MTP because of decreasing the rate of unwanted reactions [14, 85]. In the MTP reactor, water vapor is adsorbed on the surface of MFI zeolite which delays the generation of heavy hydrocarbons. In lack of feedstock water, the MFI zeolite nanosheets are poisoned by coke residues and also are deactivated via sintering the catalyst particles in highly exothermic MTP reaction [12]. Moreover, according to the reaction mechanism

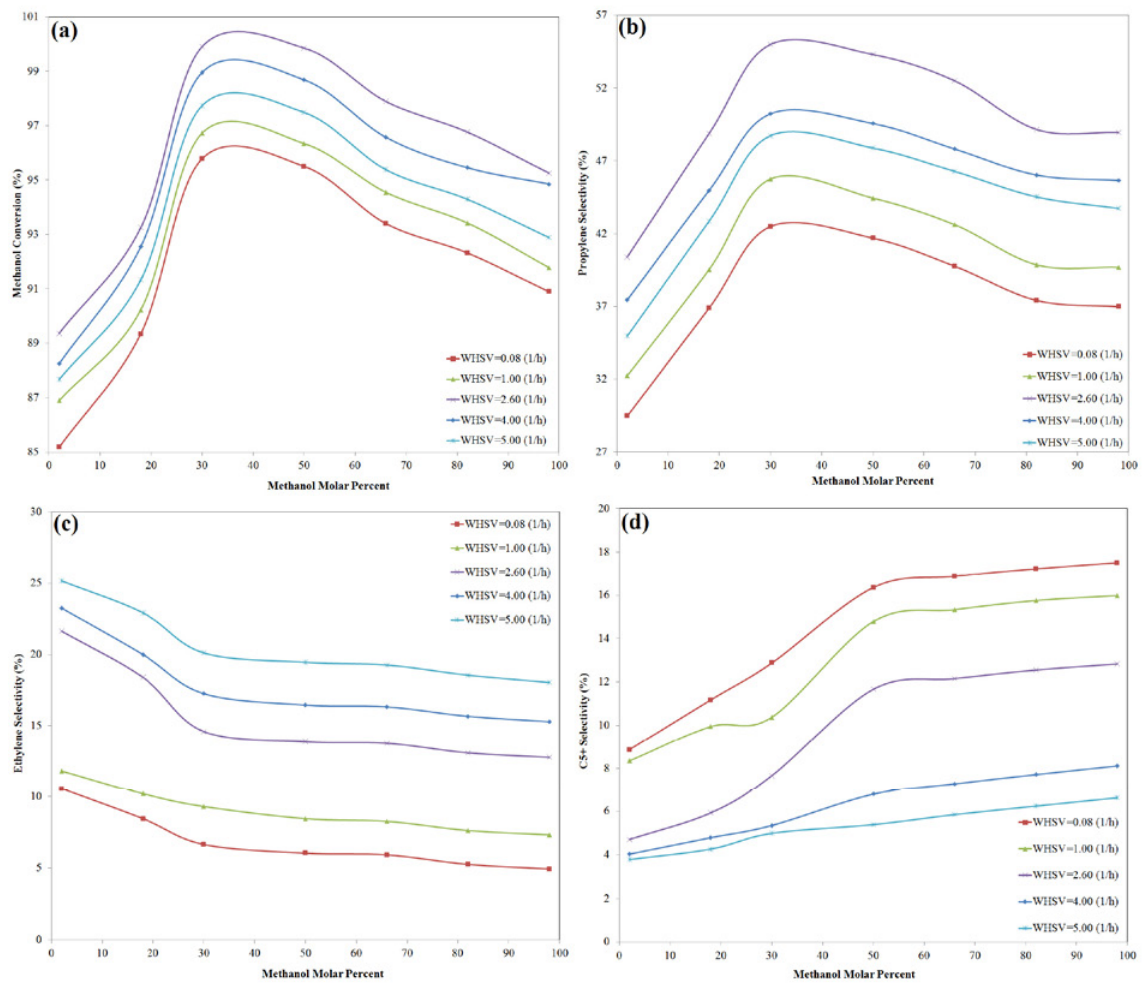


Fig. 10. Simultaneous impact of methanol molar percent and WHSV on conversion of methanol and selectivity to main MTP products at constant reaction temperature of 460 °C

which was proposed by Chen et al. [89] the ions of carbenium are produced as the intermediates during the methanol conversion. The higher methanol contents in feedstock contribute to the higher concentration of carbenium ions in the reaction zone [90]. Hence the abundant carbenium ions will react to form larger molecule hydrocarbons such as C_5^+ and coke depositions [91]. The mechanism which was suggested by Chen et al. [89] was represented in Fig. S4. Therefore, feed composition is totally a significant parameter in the MTP reaction. By using the upper contents of methanol than the optimal content in feedstock, accumulation of methanol molecules on active sites of the catalyst are extensively increased. This issue causes to enrich the concentration of carbenium ions on active sites of the catalyst which assists the formation of high carbon hydrocarbons (C_5^+). While utilizing the lower contents of methanol than the optimal composition, is uneconomic from the practical point of view because the amounts of productions are substantially declined [15].

Fig. 9 indicated the simultaneous influence of methanol molar percent in feedstock and reaction temperature on the methanol conversion and selectivity to major MTP products at constant WHSV of 2.6 h^{-1} . With respect to Fig. 9(a-c), increasing the methanol content in feedstock from 2 mol.% to 30 mol.%, maximizes the methanol conversion and also the selectivity to propylene but reduces the selectivity to ethylene. While by increasing the methanol concentration in feedstock from 30 mol.% to 98 mol.%, both of methanol conversion and propylene selectivity are declined. On the other hand, the selectivity to C_5^+ hydrocarbons is steadily intensified with increasing methanol contents in feedstock from 2 mol.% to 98 mol.%. Correspondingly, Fig. S5 demonstrated the experimental data which were achieved at specific operational conditions suggested by CCD. The similar results can be obtained by CCD examinations. Fig. S5(a-d) and Fig. S5(e) exhibited the mole percent of outlet methanol and selectivity to different MTP products in methanol molar percent in feedstock of 20% and 80% and in methanol molar percent in feedstock of 5, 50 and 95%, respectively while the reaction temperature and WHSV were kept constant. According to Fig. S5(a-d), increasing the methanol content in feedstock from 20 mol.% to 80 mol.%, favors the methanol conversion and

also the selectivity to propylene, butylene and C_5^+ hydrocarbons whereas decreases the selectivity to C_1 - C_4 alkanes and ethylene.

It is found that the greater contents of methanol in feedstock improve the formation of high carbon hydrocarbons in the MTP reaction. As it was previously discussed, in superior methanol contents in feedstock, the concentration of methanol molecules on the MFI zeolite nanosheets is notably intensified which provides the more intermediates of carbenium ions to generate the heavier hydrocarbons [32, 33, 89]. While, at the same reaction temperature and WHSV increasing water contents in feedstock intensely accelerates the production of light hydrocarbons particularly ethylene (Fig. 9c) and decreases methanol conversion, with regard to Fig. 9a. This issue probably can be attributed to the reduced amount of methanol adsorption on active acidic sites of the MFI zeolite nanosheets caused by competitive adsorption of water. The conversion of methanol is dramatically repressed at extremely low methanol/water ratio (2 mol.%). As evidenced by Fig. 9(a-b), not only the methanol conversion but also the propylene selectivity is maximized in the methanol molar percent near 30%. It is resulted that a moderate concentration of methanol molecules is needed for maximizing the methanol conversion and propylene selectivity.

The impact of methanol weight hourly space velocity

Searching for the optimal WHSV is a fundamental investigation in the MTP process. Fig. 10 represented the simultaneous effect of WHSV and methanol molar percent in feedstock on the methanol conversion and selectivity to the key MTP products at constant reaction temperature of $460 \text{ }^\circ\text{C}$. According to Fig. 10(a, b and d), increasing WHSV from 0.08 h^{-1} to 1.00 h^{-1} and further to 2.60 h^{-1} , enhances the methanol conversion and also the selectivity to propylene but reduces the selectivity to high carbon hydrocarbons (C_5^+). While by increasing the WHSV from 2.60 h^{-1} to 5.00 h^{-1} , both of methanol conversion and propylene selectivity are dropped. Although, the selectivity to ethylene is gradually strengthened with increasing WHSV from 0.08 h^{-1} to 5.00 h^{-1} (Fig. 10c). Fig. S6 revealed the empirical data which were provided at definite operational conditions advised by CCD. Fig. S6(a-d) and Fig. S6(e) revealed the mole percent of outlet methanol and the product distribution

at WHSV of 0.9 h⁻¹ and 4.1 h⁻¹ and at WHSV of 0.1, 2.5 and 4.9 h⁻¹, respectively despite the fact that in each sub-figure the reaction temperature and methanol molar percent in feedstock were held unchanged. Similar to Fig. 10, with regard to Fig. S6(a-d), growing the WHSV from 0.9 h⁻¹ to 4.1 h⁻¹, slightly reinforces the methanol conversion, enriches the selectivity to C₁-C₄ alkanes, ethylene and propylene although reduces the selectivity to butylene and C₅⁺ hydrocarbons. The lower values of WHSV's cause to increase the residence time (contact time) of feed in the MTP reactor which supplies the enough time for methanol to convert to high carbon hydrocarbons (via the methylation, hydrogen transfer and aromatization reactions). In the opposite state, the high value of WHSV decreases the feed residence time. In that case formation of light hydrocarbons is predominated. In other words, at lower contact times (higher WHSV's), ethylene and propylene have not adequate time to produce heavy alkanes and aromatics according to the consecutive dual-cycle MTP reaction mechanism (Fig. S1). This issue suppresses the aromatic cycle and the alkene cycle turns into the leading path during the MTP reaction. Hence, the MTP reaction is summarized at the light intermediates resulting more productions of light hydrocarbons [33]. These results are corresponded with the findings by Zhang et al. [69]. Fig. 10(a-b) illustrated that both of the methanol conversion and propylene selectivity were maximized at WHSV adjacent to 2.60 h⁻¹. It approved that a balanced feed velocity applicably improved the methanol conversion and propylene generation.

Optimization of operational conditions by conventional RSM coupled with CCD

The three main variables of operational conditions of the MTP process were investigated to optimize the propylene selectivity over the synthesized MFI zeolite nanosheets. Table 2 tabulated the experimental design matrix and their results for propylene selectivity at various operating conditions which were defined by CCD. Table 2 approved a reasonable agreement between the actual experimental data and predicted values.

The response values which were denoted in Table 2 were modeled by utilizing polynomial model of Eq.1. The fitted regression model is according to Eq.5.

$$y = -19.1012 + 0.2256x_1 + 0.4061x_2 + 3.9832x_3 - 0.0002x_1^2 - 0.0033x_2^2 - 0.6734x_3^2 - 0.0001x_1x_3 - 0.0021x_2x_3 \quad (5)$$

Table 4 consisted of the analysis of variance (ANOVA) results. As evidenced by Table 4, the regression F-value of 128.180 and p-value of 0.000 (p<<0.05) demonstrated that the regression model was statistically appropriate for experimental data.

Fig. S7 indicated the Pareto chart which represented the significance of main, squared and interaction terms of the regression model for the response of system. According to Fig. S7, the most significant parameter was the main factor of WHSV. The response surfaces and contour plots for propylene selectivity were shown in Fig. S8. The influence of two variables on propylene

Table 4. Analysis of variance (ANOVA) for the fit of the experimental data to the response surface model

Source of variations	Degrees of freedom	Sum of squares	Mean square	F-value	P-value
Regression	9	337.131	37.459	128.180	0.000
Linear	3	154.327	30.441	104.170	0.000
x ₁	1	113.952	44.385	151.880	0.000
x ₂	1	33.358	41.651	142.530	0.000
x ₃	1	7.016	11.730	40.140	0.000
Square	3	182.571	60.857	208.250	0.000
x ₁ ²	1	78.405	35.413	121.180	0.000
x ₂ ²	1	76.138	82.230	281.380	0.000
x ₃ ²	1	28.028	28.028	95.910	0.000
Interaction	3	0.234	0.078	0.270	0.848
x ₁ x ₂	1	0.151	0.151	0.520	0.490
x ₁ x ₃	1	0.002	0.002	0.010	0.929
x ₂ x ₃	1	0.080	0.080	0.270	0.613
Residual error	9	2.630	0.292		
Lack-of-Fit	4	2.628	0.657	1407.740	0.000
Pure error	5	0.002	0.001		
Total	18	339.761			

R²= 99.23%; R²(adj) = 98.45%



selectivity was illustrated by Fig. S8 while the third variable was kept constant at its zero level. It is worth mentioning that all of the contour plots positively illustrated a maximum region for propylene selectivity. This issue approved the proper selection of variable ranges in the experimental design. Fig. S8(a) represented that propylene selectivity was approximately

maximized in ranges of 450-500 °C and 50-70 % for reaction temperature and methanol molar percent in feedstock, respectively. Fig. S8(b) also showed that the response of system was optimized within ranges of 450-500 °C and 2.5-3.5 h⁻¹ for factors of reaction temperature and WHSV, respectively. Fig. S8(c) confirmed the optimal ranges of the variables which were obtained by Fig. S8(a) and Fig. S8(b).

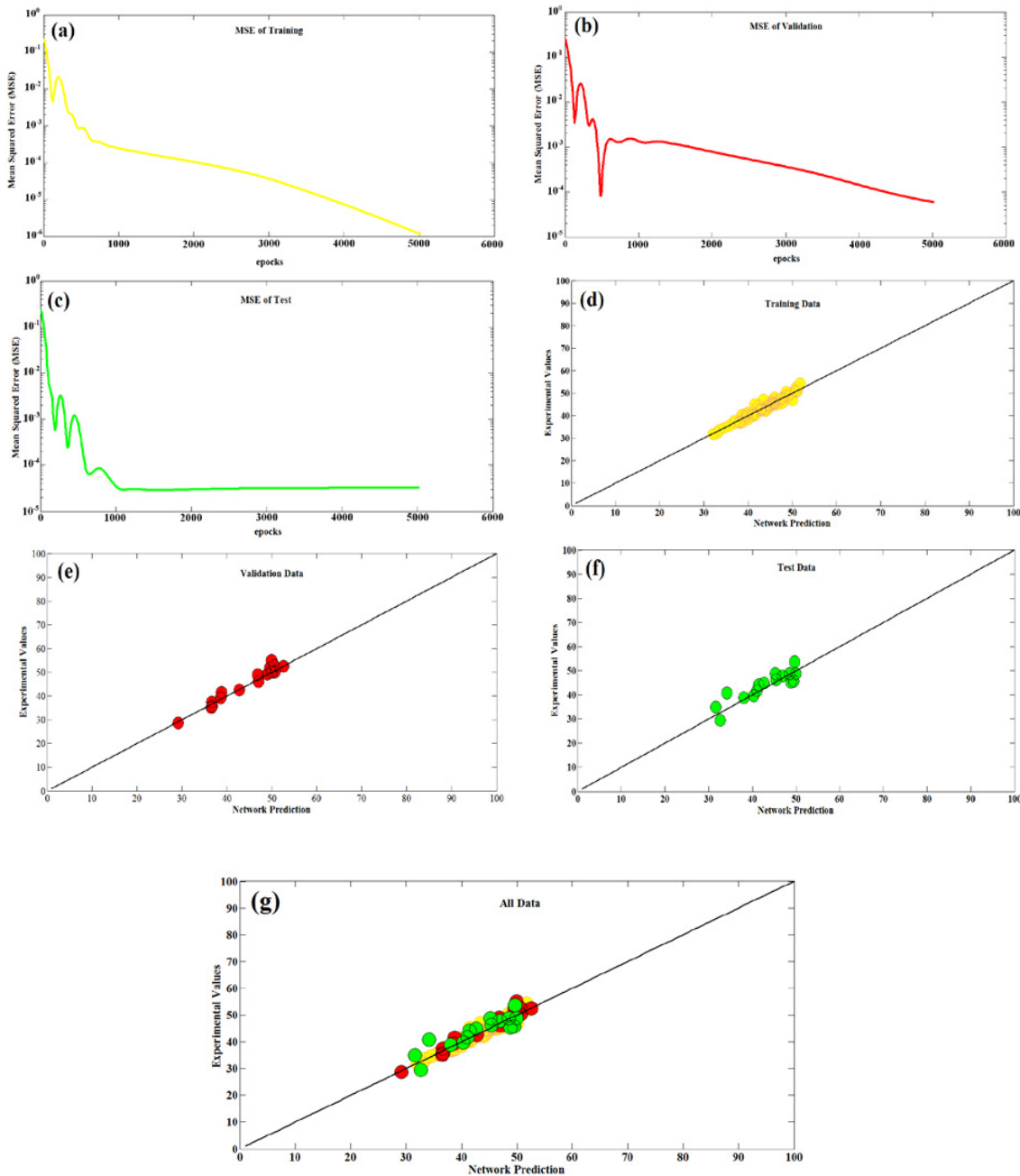


Fig. 11. Performance plots of ANN during (a) training; (b) validation and (c) test of the network. (d-g) Comparison of the experimental values with network predictions using twelve neurons in hidden layer (the optimal topology)

Optimization of operational conditions by neuro-genetic approach

As it was formerly mentioned, the databank for the ANN model was supplied by catalyst evaluations in the experimental set up of the MTP process. The databank was composed of experimental values

of propylene selectivity which were acquired at individual operating conditions determined by CCD plus the supplementary examinations at desired operational conditions which were tabulated in Table 3. An ANN topology for modeling the output of propylene selectivity was revealed by Fig. S9.

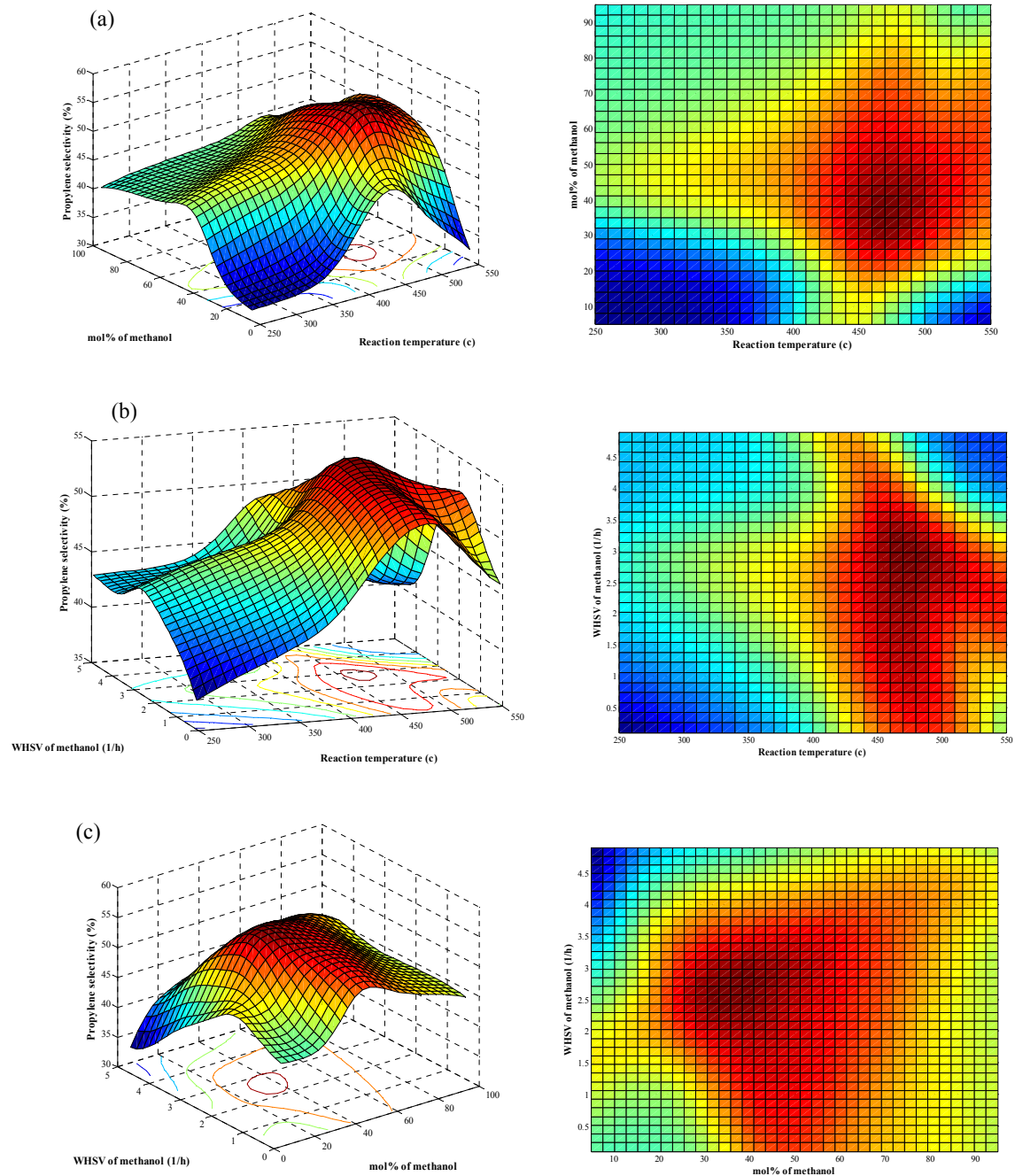


Fig. 12. The predicted propylene selectivity (%) versus reaction temperature (°C), methanol molar percent in feedstock (%) and WHSV of methanol (h^{-1}) obtained by neuro-genetic approach; the third variable was fixed at its zero level

Primarily, the optimal number of neurons in hidden layer was determined and afterwards, the optimized model was validated. The ANN modeling was started with one neuron in hidden layer and was enlarged via one by one inserting of neurons to hidden layer. For network training, testing and validating, respectively 70%, 15% and 15% of patterns were used. The value of R^2 which was calculated by Eq.2 was employed as the criterion of identifying the best qualified ANN topology (the closer the value of R^2 to 1, the more reliable that topology). According to Fig. S10, for number of twelve neurons in hidden layer not only the R^2 value was maximized for train data but also it was maximized for test data. The superior R^2 values of 0.9998 and 0.9928 for train and test data, respectively confirmed the suitable performance of ANN modeling. Hence, the topology with twelve neurons in its hidden layer was identified as the applicable topology for ANN modeling.

Fig. 11(a-c) represented the performance plots of optimal topology of ANN with twelve neurons in its hidden layer during training (Fig. 11a); validating (Fig. 11b) and testing (Fig. 11c) of the network. As evidenced by Fig. 11(a-c) the ANN model was completely matured at 5000 epochs. Moreover, the values of Mean Squared Error (MSE) of training, validation and test of the network were extremely low demonstrating the appropriate efficiency of the ANN modeling for this problem. Fig. 11(d-f) displayed the comparison between the experimental values with network prediction for training, validation and test data utilizing the optimal topology of the ANN. According to Fig. 11(g), it was deduced that the predicted values were in close agreement with the experimental data. The best and average fitness values in GA optimizer at each generation and the average distance between individuals were shown by Fig. S11a and Fig. S11b, respectively. With respect to Fig. S11, it was concluded that the GA optimizer was successfully converged at generation of 53.

The significance of the independent MTP

operating conditions on propylene selectivity was investigated on the basis of Eq.4. The Fig. S12 displayed the importance contribution of each input factor on the output factor. It was inferred that the WHSV represented the most important role among the other independent parameters. This issue was corresponded with the results of Pareto analysis of Fig. S7.

The surfaces of propylene selectivity versus two main parameters of operating conditions were achieved by neuro-genetic methodology and were depicted by Fig. 12. In each sub-Fig., the third parameter was held at its zero level. Fig. 12 verified that for the current problem the variable space was actually complicated. The combinatorial neuro-genetic methodology appropriately discovered the optimal values of the MTP operating conditions in such a complex system of variables.

Comparison of RSM-CCD and neuro-genetic techniques

For the conventional RSM-CCD, the optimal values of variables were calculated by fixing the partial derivatives of Eq.5 to zero with regard to the main factors. Whereas for the neuro-genetic approach, the optimal values of main factors were estimated by optimizer of genetic algorithm. The second and third column of Table 5 outlined the optimal values of operating conditions which were achieved by the conventional RSM-CCD and the neuro-genetic method, respectively. The propylene selectivities were expected to be 51.70% and 55.90% by conventional RSM-CCD and neuro-genetic approach, respectively. The supplementary catalyst evaluations were conducted under the optimal operating conditions. The experimental propylene selectivities were acquired around 52.00% and 55.30% at the optimal operating conditions of conventional RSM-CCD and neuro-genetic method, respectively. For both of the conventional RSM-CCD and neuro-genetic approaches, it was concluded that the

Table 5. The optimal values of major operational conditions of the MTP reaction achieved by RSM-CCD and combinatorial neuro-genetic technique

Parameter	RSM results	Neuro-genetic results
Reaction temperature (°C)	474.2	465.5
Methanol molar percent in feed (%)	57.7	34.8
WHSV of methanol (h ⁻¹)	2.8	2.6
Predicted selectivity to propylene (%)	51.70	55.90
Experimental selectivity to propylene (%)	52.00	55.30

experimental data closely were in agreement with the model predicted results. It validated the reliability of both of the conventional RSM-CCD and combinatorial neuro-genetic methods.

Via comparing the two optimization methodologies, the neuro-genetic approach has some advantages. It was realized that not only the predicted propylene selectivity, but also the experimental propylene selectivity was superior by using the results of intelligent method (neuro-genetic approach). The reason is that the neuro-genetic optimizer comprehensively searches the variable space therefore it discovers the more accurate optimal values. The optimal reaction temperature proposed by neuro-genetic method is slightly lower than the optimal reaction temperature suggested by conventional RSM-CCD and it supports energy saving. Furthermore, the optimized methanol molar percent in feedstock which was predicted by neuro-genetic method is considerably lower and it decreases the methanol consumption in the process.

Time on stream (TOS) examination at the optimal operational conditions

Fig. 13 represented the TOS examination for the MFI zeolite nanosheets at the optimal operational conditions which were proposed by combinatorial neuro-genetic approach. The propylene selectivity was more than 53% for whole TOS. In comparison with the TOS examination which was carried out in our previous work [65] over the MFI zeolite nanosheets, it was resulted that not only

the catalytic stability but also the propylene selectivity were considerably increased at the optimal operational conditions. The complete methanol conversion, propylene selectivity of 55.30%, total selectivity to light olefins of 89.90% and catalytic life-time of 101h were productively obtained over the MFI zeolite nanosheets at the optimal operational conditions. Fig. 14 illustrated the TGA profile of the spent MFI zeolite nanosheets which was examined at the optimal operational conditions. The TGA curve included two main sections. The first step of weight loss at temperature range of 20-200 °C was associated with the discharge of moisture from the catalyst sample. The second step of weight loss at temperature range of 200-800 °C was related to the combustion of coke depositions. The coke weight fractions which were deposited on the MFI zeolite nanosheets at optimal operational conditions and at operational conditions which were used in our previous work [65] were about 6.25% and 9.50%, respectively. The better catalytic life-time at the optimal operational conditions was attributed to the appropriate reaction temperature, moderate methanol concentration in feedstock and balanced WHSV which postponed the catalyst deactivation.

CONCLUSION

For the first time the major operational conditions of the MTP process were optimized by intelligent approaches. For this purpose, the special bifunctional organic surfactant of $C_{22-6-6}Br_2$ was separately synthesized and employed

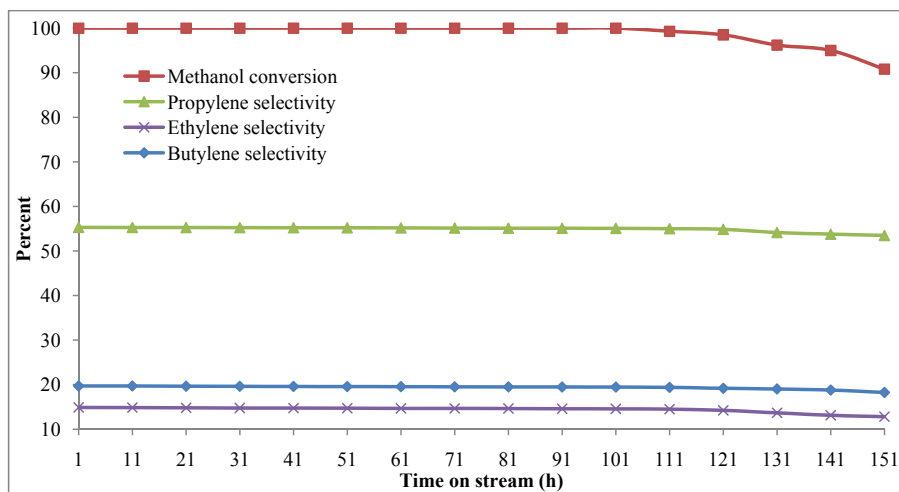


Fig. 13. TOS examination over the MFI zeolite nanosheets at the optimal operational conditions which were obtained by neuro-genetic method



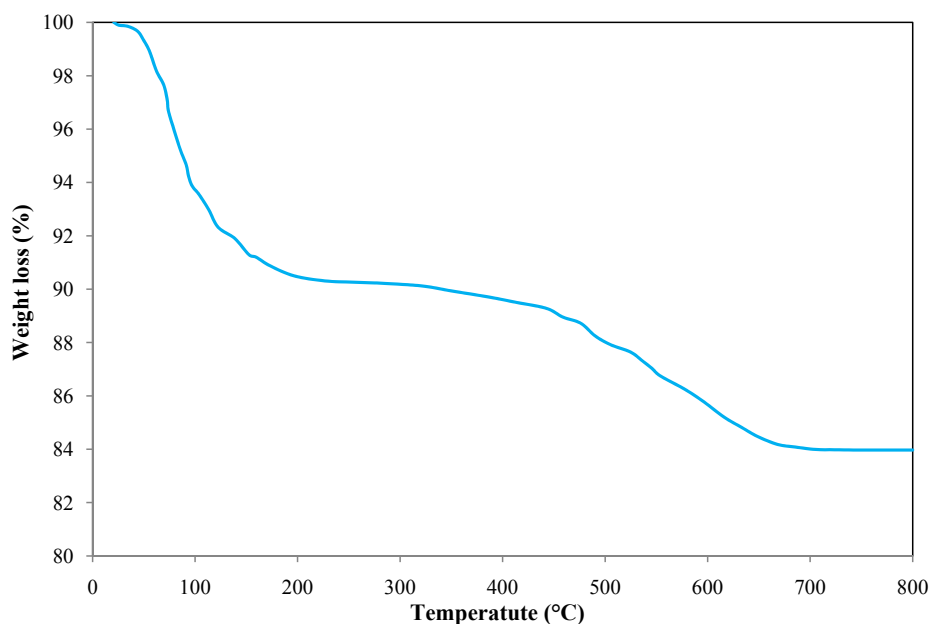


Fig. 14. TGA analysis for spent nanosheets of MFI zeolite which was examined at optimal operational conditions

as structure directing agent in the hydrothermal synthesis of the MFI zeolite nanosheets. The MTP reaction was carried out over the nanosheets of MFI zeolite at certain operational conditions which were determined by CCD and at desired operational conditions for the supplementary catalyst examinations. Three main parameters of the MTP operational conditions including reaction temperature, methanol molar percent in feedstock and methanol WHSV were considered to optimize the propylene selectivity. For systematic optimizing of operational conditions, the RSM-CCD and an intelligent method named neuro-genetic approach were applied. In order to optimize the dominant operational conditions by neuro-genetic approach, an ANN model was successfully established and then was integrated with GA to find the best operational conditions for maximizing the propylene selectivity. With respect to the optimal propylene selectivity predicted by the intelligent methods and their experimental values, it was concluded that the combinatorial neuro-genetic approach optimized the operational conditions more professionally than conventional RSM-CCD. The optimal operational conditions which were proposed by neuro-genetic approach suitably improved the catalytic life-time. The optimal operational conditions can be employed in the MTP industrial plants.

ACKNOWLEDGEMENTS

The authors gratefully acknowledge Sahand University of Technology and University of Tabriz for the financial support of the research as well as Iran Nanotechnology Initiative Council for complementary financial supports.

CONFLICT OF INTERESTS

The authors declare that there is no conflict of interests regarding the publication of this paper.

REFERENCES

1. Al-Dughaiter AS, de Lasa H. Neat dimethyl ether conversion to olefins (DTO) over HZSM-5: Effect of SiO₂/Al₂O₃ on porosity, surface chemistry, and reactivity. *Fuel*. 2014;138:52-64.
2. Zhu J, Cui Y, Nawaz Z, Wang Y, Wei F. In situ Synthesis of SAPO-34 Zeolites in Kaolin Microspheres for a Fluidized Methanol or Dimethyl Ether to Olefins Process. *Chinese Journal of Chemical Engineering*. 2010;18(6):979-87.
3. Xiang D, Yang S, Mai Z, Qian Y. Comparative study of coal, natural gas, and coke-oven gas based methanol to olefins processes in China. *Computers & Chemical Engineering*. 2015;83:176-85.
4. Baliban RC, Elia JA, Weekman V, Floudas CA. Process synthesis of hybrid coal, biomass, and natural gas to liquids via Fischer-Tropsch synthesis, ZSM-5 catalytic conversion, methanol synthesis, methanol-to-gasoline, and methanol-to-olefins/distillate technologies. *Computers & Chemical Engineering*. 2012;47:29-56.
5. Huang X, Li H, Xiao W-D, Chen D. Insight into the side reactions in methanol-to-olefin process over HZSM-5: A kinetic

- study. *Chemical Engineering Journal*. 2016;299:263-75.
6. Qi G, Xie Z, Yang W, Zhong S, Liu H, Zhang C, et al. Behaviors of coke deposition on SAPO-34 catalyst during methanol conversion to light olefins. *Fuel Processing Technology*. 2007;88(5):437-41.
 7. Jin Y, Asaoka S, Zhang S, Li P, Zhao S. Reexamination on transition-metal substituted MFI zeolites for catalytic conversion of methanol into light olefins. *Fuel Processing Technology*. 2013;115:34-41.
 8. Qi R, Fu T, Wan W, Li Z. Pore fabrication of nano-ZSM-5 zeolite by internal desilication and its influence on the methanol to hydrocarbon reaction. *Fuel Processing Technology*. 2017;155:191-9.
 9. Dubois DR, Obrzut DL, Liu J, Thundimadathil J, Adekkanattu PM, Guin JA, et al. Conversion of methanol to olefins over cobalt-, manganese- and nickel-incorporated SAPO-34 molecular sieves. *Fuel Processing Technology*. 2003;83(1-3):203-18.
 10. Soundararajan S, Dalai AK, Berruti F. Modeling of methanol to olefins (MTO) process in a circulating fluidized bed reactor. *Fuel*. 2001;80(8):1187-97.
 11. Rostamizadeh M, Taeb A. Highly selective Me-ZSM-5 catalyst for methanol to propylene (MTP). *Journal of Industrial and Engineering Chemistry*. 2015;27:297-306.
 12. Rostamizadeh M, Yaripour F. Bifunctional and bimetallic Fe/ZSM-5 nanocatalysts for methanol to olefin reaction. *Fuel*. 2016;181:537-46.
 13. Wu W, Guo W, Xiao W, Luo M. Dominant reaction pathway for methanol conversion to propene over high silicon H-ZSM-5. *Chemical Engineering Science*. 2011;66(20):4722-32.
 14. Liu J, Zhang C, Shen Z, Hua W, Tang Y, Shen W, et al. Methanol to propylene: Effect of phosphorus on a high silica HZSM-5 catalyst. *Catalysis Communications*. 2009;10(11):1506-9.
 15. Mei C, Wen P, Liu Z, Liu H, Wang Y, Yang W, et al. Selective production of propylene from methanol: Mesoporosity development in high silica HZSM-5. *Journal of Catalysis*. 2008;258(1):243-9.
 16. Hadi N, Niaei A, Nabavi SR, Navaei Shirazi M, Alizadeh R. Effect of second metal on the selectivity of Mn/H-ZSM-5 catalyst in methanol to propylene process. *Journal of Industrial and Engineering Chemistry*. 2015;29:52-62.
 17. Yaripour F, Shariatnia Z, Sahebdehfar S, Irandoukht A. Conventional hydrothermal synthesis of nanostructured H-ZSM-5 catalysts using various templates for light olefins production from methanol. *Journal of Natural Gas Science and Engineering*. 2015;22:260-9.
 18. Guo W, Wu W, Luo M, Xiao W. Modeling of diffusion and reaction in monolithic catalysts for the methanol-to-propylene process. *Fuel Processing Technology*. 2013;108:133-8.
 19. Li M, Zhou Y, Oduro IN, Fang Y. Comparative study on the catalytic conversion of methanol and propanal over Ga/ZSM-5. *Fuel*. 2016;168:68-75.
 20. Huang X, Li H, Li H, Xiao W-D. A computationally efficient multi-scale simulation of a multi-stage fixed-bed reactor for methanol to propylene reactions. *Fuel Processing Technology*. 2016;150:104-16.
 21. Ortiz-Espinoza AP, Noureldin MMB, El-Halwagi MM, Jiménez-Gutiérrez A. Design, simulation and techno-economic analysis of two processes for the conversion of shale gas to ethylene. *Computers & Chemical Engineering*. 2017;107:237-46.
 22. Xiaolong G, Botong L, Xigang Y, Yiqing L, Kuo-Ksong Y. Application of the dividing wall column to olefin separation in fluidization methanol to propylene (FMTP) process. *Chinese Journal of Chemical Engineering*. 2017;25(8):1069-78.
 23. Wu W, Guo W, Xiao W, Luo M. Methanol conversion to olefins (MTO) over H-ZSM-5: Evidence of product distribution governed by methanol conversion. *Fuel Processing Technology*. 2013;108:19-24.
 24. Zhuang Y-Q, Chen X-M, Luo Z-H, Xiao J. CFD-DEM modeling of gas-solid flow and catalytic MTO reaction in a fluidized bed reactor. *Computers & Chemical Engineering*. 2014;60:1-16.
 25. Ahmadvpour J, Taghizadeh M. Catalytic conversion of methanol to propylene over high-silica mesoporous ZSM-5 zeolites prepared by different combinations of mesogenous templates. *Journal of Natural Gas Science and Engineering*. 2015;23:184-94.
 26. Ahmadvpour J, Taghizadeh M. Selective production of propylene from methanol over high-silica mesoporous ZSM-5 zeolites treated with NaOH and NaOH/tetrapropylammonium hydroxide. *Comptes Rendus Chimie*. 2015;18(8):834-47.
 27. Jang H-G, Min H-K, Hong SB, Seo G. Tetramethylbenzenium radical cations as major active intermediates of methanol-to-olefin conversions over phosphorus-modified HZSM-5 zeolites. *Journal of Catalysis*. 2013;299:240-8.
 28. Han L, Jiang X-G, Lu T-L, Wang B-S, Xu J, Zhan Y-Z, et al. Preparation of composite zeolites in polymer hydrogels and their catalytic performances in the methanol-to-olefin reaction. *Fuel Processing Technology*. 2017;165:87-93.
 29. Huang X, Li X-G, Li H, Xiao W-D. High-performance HZSM-5/cordierite monolithic catalyst for methanol to propylene reaction: A combined experimental and modelling study. *Fuel Processing Technology*. 2017;159:168-77.
 30. Hadi N, Niaei A, Nabavi S, Farzi A. Kinetic Study of Methanol to Propylene Process on High Silica H-ZSM5 Catalyst. *Iran J Chem Eng*, 2013;10(4):17.
 31. Ghavipour M, Behbahani RM, Moradi GR, Soleimanimehr A. Methanol dehydration over alkali-modified H-ZSM-5; effect of temperature and water dilution on products distribution. *Fuel*. 2013;113:310-7.
 32. Taheri Najafabadi A, Fatemi S, Sohrabi M, Salmasi M. Kinetic modeling and optimization of the operating condition of MTO process on SAPO-34 catalyst. *Journal of Industrial and Engineering Chemistry*. 2012;18(1):29-37.
 33. Hajimirzaee S, Ainte M, Soltani B, Behbahani RM, Leeke GA, Wood J. Dehydration of methanol to light olefins upon zeolite/alumina catalysts: Effect of reaction conditions, catalyst support and zeolite modification. *Chemical Engineering Research and Design*. 2015;93:541-53.
 34. Estahbanati MRK, Feilizadeh M, Iliuta MC. Photocatalytic valorization of glycerol to hydrogen: Optimization of operating parameters by artificial neural network. *Applied Catalysis B: Environmental*. 2017;209:483-92.
 35. Chamkalani A, Mae'soumi A, Sameni A. An intelligent approach for optimal prediction of gas deviation factor using particle swarm optimization and genetic algorithm. *Journal of Natural Gas Science and Engineering*. 2013;14:132-43.
 36. Khalilpourmeymandi H, Mirvakili A, Rahimpour MR, Shariati A. Application of response surface methodology for optimization of purge gas recycling to an industrial reactor

- for conversion of CO₂ to methanol. Chinese Journal of Chemical Engineering. 2017;25(5):676-87.
37. Jiang B, Zhang F, Sun Y, Zhou X, Dong J, Zhang L. Modeling and optimization for curing of polymer flooding using an artificial neural network and a genetic algorithm. Journal of the Taiwan Institute of Chemical Engineers. 2014;45(5):2217-24.
 38. Omata K, Kobayashi Y, Yamada M. Artificial neural network-aided design of Co/SrCO₃ catalyst for preferential oxidation of CO in excess hydrogen. Catalysis Today. 2006;117(1-3):311-5.
 39. Umegaki T, Masuda A, Omata K, Yamada M. Development of a high performance Cu-based ternary oxide catalyst for oxidative steam reforming of methanol using an artificial neural network. Applied Catalysis A: General. 2008;351(2):210-6.
 40. Oskoui SA, Niaei A, Tseng H-H, Salari D, Izadkhan B, Hosseini SA. Modeling Preparation Condition and Composition-Activity Relationship of Perovskite-Type La_xSr_{1-x}Fe_yCo_{1-y}O₃ Nano Catalyst. ACS Combinatorial Science. 2013;15(12):609-21.
 41. Izadkhan B, Nabavi SR, Niaei A, Salari D, Mahmuodi Badiki T, Çaylak N. Design and optimization of Bi-metallic Ag-ZSM5 catalysts for catalytic oxidation of volatile organic compounds. Journal of Industrial and Engineering Chemistry. 2012;18(6):2083-91.
 42. Niaei A, Badiki TM, Nabavi SR, Salari D, Izadkhan B, Çaylak N. Neuro-genetic aided design of modified H-ZSM-5 catalyst for catalytic conversion of methanol to gasoline range hydrocarbons. Journal of the Taiwan Institute of Chemical Engineers. 2013;44(2):247-56.
 43. Mousavi SM, Niaei A, Salari D, Panahi PN, Samandari M. Modelling and optimization of Mn/activate carbon nanocatalysts for NO reduction: comparison of RSM and ANN techniques. Environmental Technology. 2013;34(11):1377-84.
 44. Hosseini SA, Niaei A, Salari D, Nabavi SR. Modeling and optimization of combustion process of 2-propanol over perovskite-type LaMnCo_{1-y}O₃ nanocatalysts by an unreplicated experimental design with mixture-process variables and genetic algorithm methodology. Journal of the Taiwan Institute of Chemical Engineers. 2014;45(1):85-91.
 45. Panahi PN, Salari D, Niaei A, Mousavi SM. NO reduction over nanostructure M-Cu/ZSM-5 (M: Cr, Mn, Co and Fe) bimetallic catalysts and optimization of catalyst preparation by RSM. Journal of Industrial and Engineering Chemistry. 2013;19(6):1793-9.
 46. Hosseini SA, Niaei A, Salari D, Jodaei A. Gas Phase Oxidation of Toluene and Ethyl Acetate over Proton and Cobalt Exchanged ZSM-5 Nano Catalysts- Experimental Study and ANN Modeling. Bulletin of the Korean Chemical Society. 2010;31(4):808-14.
 47. Khataee AR, Fathinia M, Zarei M, Izadkhan B, Joo SW. Modeling and optimization of photocatalytic/photoassisted-electro-Fenton like degradation of phenol using a neural network coupled with genetic algorithm. Journal of Industrial and Engineering Chemistry. 2014;20(4):1852-60.
 48. Assefi P, Ghaedi M, Ansari A, Habibi MH, Momeni MS. Artificial neural network optimization for removal of hazardous dye Eosin Y from aqueous solution using Co₂O₃-NP-AC: Isotherm and kinetics study. Journal of Industrial and Engineering Chemistry. 2014;20(5):2905-13.
 49. Karimi H, Ghaedi M. Application of artificial neural network and genetic algorithm to modeling and optimization of removal of methylene blue using activated carbon. Journal of Industrial and Engineering Chemistry. 2014;20(4):2471-6.
 50. Zonouz PR, Niaei A, Tarjomannejad A. Modeling and optimization of toluene oxidation over perovskite-type nanocatalysts using a hybrid artificial neural network-genetic algorithm method. Journal of the Taiwan Institute of Chemical Engineers. 2016;65:276-85.
 51. Naeem S, Shahhosseini S, Ghaemi A. Simulation of CO₂ capture using sodium hydroxide solid sorbent in a fluidized bed reactor by a multi-layer perceptron neural network. Journal of Natural Gas Science and Engineering. 2016;31:305-12.
 52. Luo J, Lin W, Cai X, Li J. Optimization of Fermentation Media for Enhancing Nitrite-oxidizing Activity by Artificial Neural Network Coupling Genetic Algorithm. Chinese Journal of Chemical Engineering. 2012;20(5):950-7.
 53. Sedighi M, Towfighi J. Methanol conversion over SAPO-34 catalysts; Systematic study of temperature, space-time, and initial gel composition on product distribution and stability. Fuel. 2015;153:382-92.
 54. Hadi N, Niaei A, Nabavi SR, Alizadeh R, Shirazi MN, Izadkhan B. An intelligent approach to design and optimization of M-Mn/H-ZSM-5 (M: Ce, Cr, Fe, Ni) catalysts in conversion of methanol to propylene. Journal of the Taiwan Institute of Chemical Engineers. 2016;59:173-85.
 55. Adib H, Haghbakhsh R, Saidi M, Takassi MA, Sharifi F, Koolivand M, et al. Modeling and optimization of Fischer-Tropsch synthesis in the presence of Co (III)/Al₂O₃ catalyst using artificial neural networks and genetic algorithm. Journal of Natural Gas Science and Engineering. 2013;10:14-24.
 56. Ghorbani B, Ziabasharhagh M, Amidpour M. A hybrid artificial neural network and genetic algorithm for predicting viscosity of Iranian crude oils. Journal of Natural Gas Science and Engineering. 2014;18:312-23.
 57. Choi M, Na K, Kim J, Sakamoto Y, Terasaki O, Ryoo R. Stable single-unit-cell nanosheets of zeolite MFI as active and long-lived catalysts. Nature. 2009;461(7261):246-9.
 58. Na K, Choi M, Park W, Sakamoto Y, Terasaki O, Ryoo R. Pillared MFI Zeolite Nanosheets of a Single-Unit-Cell Thickness. Journal of the American Chemical Society. 2010;132(12):4169-77.
 59. Na K, Park W, Seo Y, Ryoo R. Disordered Assembly of MFI Zeolite Nanosheets with a Large Volume of Intersheet Mesopores. Chemistry of Materials. 2011;23(5):1273-9.
 60. Machoke AG, Knoke IY, Lopez-Orozco S, Schmiele M, Selvam T, Marthala VRR, et al. Synthesis of multilamellar MFI-type zeolites under static conditions: The role of gel composition on their properties. Microporous and Mesoporous Materials. 2014;190:324-33.
 61. Kim Y, Kim J-C, Jo C, Kim T-W, Kim C-U, Jeong S-Y, et al. Structural and physicochemical effects of MFI zeolite nanosheets for the selective synthesis of propylene from methanol. Microporous and Mesoporous Materials. 2016;222:1-8.
 62. Schick J, Daou TJ, Caultel P, Paillaud J-L, Patarin J, Mangold-Callarec C. Surfactant-modified MFI nanosheets: a high capacity anion-exchanger. Chem Commun. 2011;47(3):902-4.
 63. Park W, Yu D, Na K, Jelfs KE, Slater B, Sakamoto Y, et

- al. Hierarchically Structure-Directing Effect of Multi-Ammonium Surfactants for the Generation of MFI Zeolite Nanosheets. *Chemistry of Materials*. 2011;23(23):5131-7.
64. Hu S, Shan J, Zhang Q, Wang Y, Liu Y, Gong Y, et al. Selective formation of propylene from methanol over high-silica nanosheets of MFI zeolite. *Applied Catalysis A: General*. 2012;445-446:215-20.
 65. Hadi N, Alizadeh R, Niaei A. Selective production of propylene from methanol over nanosheets of metal-substituted MFI zeolites. *Journal of Industrial and Engineering Chemistry*. 2017;54:82-97.
 66. Park T-Y, Froment GF. Kinetic Modeling of the Methanol to Olefins Process. 1. Model Formulation. *Industrial & Engineering Chemistry Research*. 2001;40(20):4172-86.
 67. Alwahabi SM, Froment GF. Single Event Kinetic Modeling of the Methanol-to-Olefins Process on SAPO-34. *Industrial & Engineering Chemistry Research*. 2004;43(17):5098-111.
 68. Bjorgen M, Svelle S, Joensen F, Nerlov J, Kolboe S, Bonino F, et al. Conversion of methanol to hydrocarbons over zeolite H-ZSM-5: On the origin of the olefinic species. *Journal of Catalysis*. 2007;249(2):195-207.
 69. Zhang M, Xu S, Wei Y, Li J, Wang J, Zhang W, et al. Changing the balance of the MTO reaction dual-cycle mechanism: Reactions over ZSM-5 with varying contact times. *Chinese Journal of Catalysis*. 2016;37(8):1413-22.
 70. Haw JF, Nicholas JB, Song W, Deng F, Wang Z, Xu T, et al. Roles for Cyclopentenyl Cations in the Synthesis of Hydrocarbons from Methanol on Zeolite Catalyst HZSM-5. *Journal of the American Chemical Society*. 2000;122(19):4763-75.
 71. Xu T, Barich DH, Goguen PW, Song W, Wang Z, Nicholas JB, et al. Synthesis of a Benzenium Ion in a Zeolite with Use of a Catalytic Flow Reactor. *Journal of the American Chemical Society*. 1998;120(16):4025-6.
 72. Xu S, Zheng A, Wei Y, Chen J, Li J, Chu Y, et al. Direct Observation of Cyclic Carbenium Ions and Their Role in the Catalytic Cycle of the Methanol-to-Olefin Reaction over Chabazite Zeolites. *Angewandte Chemie International Edition*. 2013;52(44):11564-8.
 73. Li J, Wei Y, Qi Y, Tian P, Li B, He Y, et al. Conversion of methanol over H-ZSM-22: The reaction mechanism and deactivation. *Catalysis Today*. 2011;164(1):288-92.
 74. Li J, Wei Y, Liu G, Qi Y, Tian P, Li B, et al. Comparative study of MTO conversion over SAPO-34, H-ZSM-5 and H-ZSM-22: Correlating catalytic performance and reaction mechanism to zeolite topology. *Catalysis Today*. 2011;171(1):221-8.
 75. Ilias S, Khare R, Malek A, Bhan A. A descriptor for the relative propagation of the aromatic- and olefin-based cycles in methanol-to-hydrocarbons conversion on H-ZSM-5. *Journal of Catalysis*. 2013;303:135-40.
 76. Ilias S, Bhan A. Tuning the selectivity of methanol-to-hydrocarbons conversion on H-ZSM-5 by co-processing olefin or aromatic compounds. *Journal of Catalysis*. 2012;290:186-92.
 77. Thouchprasitchai N, Luengnaruemitchai A, Pongstabodee S. Statistical optimization by response surface methodology for water-gas shift reaction in a H₂-rich stream over Cu-Zn-Fe composite-oxide catalysts. *Journal of the Taiwan Institute of Chemical Engineers*. 2011;42(4):632-9.
 78. Chakraborty R, RoyChowdhury D. Optimization of biological-hydroxyapatite supported iron catalyzed methyl oleate synthesis using response surface methodology. *Journal of the Taiwan Institute of Chemical Engineers*. 2014;45(1):92-100.
 79. Montgomery DC. *Design and analysis of experiments*: John Wiley & Sons; 2008.
 80. Zi W, Peng J, Zhang X, Zhang L, Liu J. Optimization of waste tobacco stem expansion by microwave radiation for biomass material using response surface methodology. *Journal of the Taiwan Institute of Chemical Engineers*. 2013;44(4):678-85.
 81. Goh ATC. Back-propagation neural networks for modeling complex systems. *Artificial Intelligence in Engineering*. 1995;9(3):143-51.
 82. Treacy MM, Higgins JB. *Collection of Simulated XRD Powder Patterns for Zeolites Fifth (5th) Revised Edition*: Elsevier; 2007.
 83. Espinoza RL. Oligomerization vs. methylation of propene in the conversion of dimethyl ether (or methanol) to hydrocarbons. *Industrial & Engineering Chemistry Product Research and Development*. 1984;23(3):449-52.
 84. Svelle S, Joensen F, Nerlov J, Olsbye U, Lillerud K-P, Kolboe S, et al. Conversion of Methanol into Hydrocarbons over Zeolite H-ZSM-5: Ethene Formation Is Mechanistically Separated from the Formation of Higher Alkenes. *Journal of the American Chemical Society*. 2006;128(46):14770-1.
 85. Hadi N, Niaei A, Nabavi S, Farzi A, Navaei Shirazi M. Development of a new kinetic model for methanol to propylene process on Mn/H-ZSM-5 catalyst. *Chem Biochem Eng Q*, 2014;28(1):53-63.
 86. Möller KP, Böhringer W, Schnitzler AE, van Steen E, O'Connor CT. The use of a jet loop reactor to study the effect of crystal size and the co-feeding of olefins and water on the conversion of methanol over HZSM-5. *Microporous and Mesoporous Materials*. 1999;29(1-2):127-44.
 87. Stöcker M. Methanol-to-hydrocarbons: catalytic materials and their behavior. *Microporous and Mesoporous Materials*. 1999;29(1-2):3-48.
 88. Dehertog WJH, Froment GF. Production of light alkenes from methanol on ZSM-5 catalysts. *Applied Catalysis*. 1991;71(1):153-65.
 89. Chen D, Rebo HP, Grønvold A, Moljord K, Holmen A. Methanol conversion to light olefins over SAPO-34: kinetic modeling of coke formation. *Microporous and Mesoporous Materials*. 2000;35-36:121-35.
 90. Mihail R, Straja S, Maria G, Musca G, Pop G. A kinetic model for methanol conversion to hydrocarbons. *Chemical Engineering Science*. 1983;38(9):1581-91.
 91. Chang CD. A kinetic model for methanol conversion to hydrocarbons. *Chemical Engineering Science*. 1980;35(3):619-22.